JOURNAL OF GEOPHYSICAL RESEARCH, VOL. 106, NO. D17, PAGES 20,311–20,332, SEPTEMBER 16, 2001

Transport and direct radiative forcing of carbonaceous and sulfate aerosols in the GISS GCM

Dorothy Koch

NASA Goddard Institute for Space Studies, Columbia University, New York

Abstract. We simulate the major anthropogenic aerosols, sulfate, organic carbon and black carbon, in the Goddard Institute for Space Studies General Circulation Model (GISS GCM), and examine their transport, relative abundances, and direct radiative forcing. Both present-day and projected future emissions are used, as provided by the IPCC SRES (A2) scenarios for 2030 and 2100. We consider the sensitivity of the black carbon distribution to the treatment of its solubility and allow solubility to depend upon exposure to gas phase production of sulfuric acid (case S), or time (case A), or a fixed rate (case C). We show that all three approaches can be tuned to give reasonable agreement with present-day observations. However, case S has higher black carbon in the arctic winter, owing to reduced SO_2 oxidation and black carbon solubility. This improves upon the arctic deficiency in previous models, though may be somewhat excessive in this model. We also show that with a different ratio of sulfur/carbonaceous emissions, the case S mechanism can give significantly different results compared to the other mechanisms. Thus, in the 2100 simulation, with reduced sulfur and increased black carbon emissions, the black carbon burden is ~13% higher and the direct radiative forcing is ~40% higher in case S compared to the other cases. We consider the relative abundances of carbonaceous and sulfate aerosols in different regions. In the current simulations, carbonaceous aerosols exceed sulfate at the surface in Asia and much of Europe and throughout the column in biomass burning regions. We show that the model ratio of carbonaceous to sulfate aerosols increases with altitude over many oceanic regions, especially in summertime, as was observed during the Tropospheric Aerosol Radiative Forcing Observational Experiment campaign; however, over land and during other seasons the ratio generally decreases with altitude. The (present day) direct radiative forcings for externally mixed (case A) black carbon, organic carbon, and sulfate are calculated to be 0.35, -0.30, and -0.65 W/m^2, respectively. In the 2100 simulation these forcings are 0.89, -0.64, and -0.54 W/m^2, respectively. The net anthropogenic aerosol global average forcing seasonality inverts between the current and future simulations: the forcing is most negative in (Northern Hemisphere) summertime in 2000 but is least negative or even positive during (NH) summer in 2100; this inversion is more extreme in the Northern Hemisphere.

1. Introduction

Tropospheric aerosols are recognized to be among the most important, but least certain, elements of climate change. Anthropogenic activity, including the burning of fossil fuels and biomass, have increased the Earth's aerosol load, primarily in the form of sulfate and carbonaceous aerosols. Although early studies often assumed that sulfate had the dominant anthropogenic aerosol influence, recent studies have contended that carbonaceous aerosols may be as, or more, important. Aerosols impact climate in at least three ways. Sulfate scatters incoming solar radiation, thereby cooling the Earth's surface; carbonaceous aerosols can scatter or absorb radiation and thus have the potential of warming or cooling the atmosphere. Both aerosol types may act as cloud condensation nuclei (CCN), thus perturbing cloud cover and cloud properties (indirect effect). Also both may influence tropospheric chemistry, as they act as sites for heterogeneous chemical reactions. Thus these anthropogenic aerosols may influence climate directly by scattering and absorbing radiation and indirectly by acting as CCN and affecting atmospheric chemistry.

Modeling of these aerosols, and therefore their climate effects, is hampered by a number of uncertainties. Current sources are improving, though still uncertain

Paper number 2001JD900038.
0148-0227/01/2001JD900038$09.00

to at least a factor of 2 [e.g., *Cooke et al.,* 1999]; moreover, we are limited in our knowledge of how they have evolved since preindustrial times and obviously even more limited in how we may project emissions into the future. Carbonaceous aerosols, including organic carbon species and the absorptive component, black carbon, include a large variety of chemical and structural forms, many of which are not even known. Each form, if modeled precisely, would have its own source, chemical behavior, solubility, and radiative property. Furthermore, aerosols are often observed to be internally mixed, that is, each particle typically contains multiple species. If this were modeled correctly, each particle would have its own solubility and radiative properties, dependent on size, composition and structure. Considering these uncertainties, the modeling of aerosols remains fairly primitive and in need of further development.

Most aerosol modeling studies to date have focused on single aerosol types. In order to address the uncertainties listed above and to study the interactions of aerosol types, modeling must now include multiple aerosol species. In this study, we consider the primary anthropogenic aerosols: we add black and organic carbon to the sulfate simulation from *Koch et al.* [1999] and simulate all species together in a general circulation model. Many aspects of the carbonaceous model remain crude; unfortunately, the current quality of observations severely limit model validation and therefore make it difficult to justify more sophisticated modeling, as we will demonstrate.

Our aim is to produce a model that provides reasonable agreement (or at least minimal bias) compared with available measurements and then use it to examine some issues of interest. We will consider the relative "importance" of sulfate and carbonaceous aerosols. Some recent campaigns, such as TARFOX (off the eastern coast of North America) have found that carbonaceous aerosols are at least as abundant as sulfates and that their importance increases with altitude. We will use our model to consider the degree to which this is a global phenomenon.

One difficulty in the modeling of carbonaceous aerosols is the treatment of solubility and precipitation scavenging. This is not so problematic for sulfate, since it is highly soluble; thus scavenging of sulfate can be modeled based on physical principles. However, carbonaceous aerosol solubility has been found to span a considerable range [e.g., *Saxena and Hildemann,* 1996], depending on a number of factors such as composition, mixture with or coating by soluble species, and physical structure. Precise and physical modeling of this is prohibitive and beyond current understanding of aerosol behavior. The most straightforward approach is to adjust scavenging amount so that the model (with current emissions) gives minimal bias compared with current observations. Unfortunately, there is no guarantee that such a model, tuned to current data, will be accurate in past and future climate studies, since the factors causing solubility also change.

We will therefore consider in some detail the treatment of black carbon (BC) solubility. We limit the sensitivity study to BC and not organic carbon (OC), since the source is better constrained and more BC data are available. Some previous studies have argued that BC may be insoluble when it is emitted and then become more soluble as it "ages". Its increased solubility may be due to exposure to the oxidizing atmosphere, or coating by a soluble species such as sulfuric acid or gaseous organic carbon (such coating may occur initially, if both species are emitted together). Previous modeling studies [*Cooke and Wilson,* 1996; *Cooke et al.,* 1999] have modeled this by allowing BC to become soluble after some aging period that is applied globally. We will consider three treatments of BC solubility. In one, we use the aging approach of *Cooke and Wilson* [1996]. In another, we allow solubility to occur after exposure to gas phase SO_2 oxidation (to approximate coating by sulfuric acid). Finally we use a simple, fixed solubility rate.

We will look at the global distributions and (direct) radiative forcings of sulfate, BC and OC for both present and future (using emissions scenarios from the IPCC model intercomparison). We will consider the behaviors of the three BC solubility approaches in the future model simulations. Of particular interest is the approach which allows BC solubility to depend on SO_2 oxidation, since the relative levels of sulfur/BC emissions are projected to evolve from 8 to 9 to 3 Tg S/Tg C in the years 2000, 2030, and 2100, respectively. Thus we may see how changes in sulfuric acid availability impact the BC distribution and the radiative forcing. From this we may infer the degree to which ignorance about BC solubility mechanisms generates uncertainty in the prediction of future climate.

2. Model Description

We simulate three aerosol species, sulfate, black carbon, and organic carbon, online in the Goddard Institute for Space Studies General Circulation Model (GISS GCM), version II-prime. The carbonaceous aerosols have been added to the sulfur model of *Koch et al.* [1999], which also simulates prognostic species dimethylsulfide (DMS), methanesulfonic acid (MSA), SO_2, and H_2O_2. Model resolution is 4° latitude by 5° longitude and nine vertical sigma layers, with one to two layers in the stratosphere. We use current climatological fixed sea surface temperatures. In comparison with the older version of the GISS GCM [*Hansen et al.,* 1983] this version has improved subroutines for the boundary layer, convection, land surface, and a cloud liquid water budget and uses the quadratic upstream scheme for heat and moisture advection as well as a fourth-order advection scheme. Details on the various components are discussed or referenced by *Rind and Lerner* [1996]. The

masses of the chemical species are also transported using the quadratic upstream scheme (aerosol size distribution is not simulated).

The sources are from the Intergovernmental Panel on Climate Change (IPCC) Special Report on Emissions Scenarios (SRES), scenario A2 for current (2000) and future (2030 and 2100) emissions of SO_2 and carbonaceous aerosols. Scenario A2 was chosen for the IPCC model intercomparison because it projects a significant increase in sulfur emissions (by a factor of 1.6) for 2030, followed by a decrease in 2100. Carbonaceous aerosols, which are scaled to projected changes in CO, increase by a factor of 1.3 in 2030 and then by another factor of 1.8 in 2100. Thus we are able to see the effects of both an increase and decrease in the ratio of sulfur/carbonaceous emission compared with present-day conditions. For the present-day simulations the IPCC inventory used carbonaceous aerosol biomass emissions from *Liousse et al.* [1996], BC fossil fuel emissions from *Penner et al.* [1993]; OC fossil fuel emissions were assumed to be a factor of 4 times the BC emissions. The recent industrial emissions inventory for carbonaceous aerosols from *Cooke et al.* [1999] is probably more accurate than that used here; however, we use the IPCC inventory in order to work with future as well as current emissions. Industrial SO_2 emissions are from IPCC [*Nakicenovic et al.*, 2000]. In the 2000 simulation these are similar in magnitude to the Global Emissions Inventory Activity inventory for 1985 used by *Koch et al.* [1999]; however, the IPCC 2000 source has greater emissions in Southeast Asia. Natural sulfur emissions include DMS from *Kettle et al.* [1999] (using a higher sea-air-transfer rate than by *Koch et al.* [1999]) and steady volcanic emissions (from GEIA) of SO_2. A natural organic carbon source is derived from terpenes [*Guenther et al.*, 1995], using a 5% yield rate [*Liousse et al.*, 1996].

This study makes use of the dry and wet deposition schemes from *Koch et al.* [1999]. These schemes and the sulfur chemistry are summarized here briefly. The sulfur model includes transport of species SO_2, DMS, sulfate, H_2O_2, and MSA. Gas-phase chemistry includes oxidation of DMS by NO_3 and OH to form SO_2, oxidation of SO_2 by OH to form sulfate, formation of H_2O_2 by HO_2, and destruction of H_2O_2 by photolysis and reaction with OH. The oxidants were imported from other global simulations and scaled by daylight to give a diurnal cycle. Heterogeneous chemistry includes the uptake of SO_2 and H_2O_2 into cloud droplets and reaction to form sulfate. Henry's law is used to determine gas dissolution into the cloud droplets. Dry deposition of the aerosols and gases is done using a resistance in series scheme, making use of GCM-generated surface momentum and heat fluxes.

In large-scale (stratiform) clouds, dissolved gases and aerosols are scavenged assuming a first-order removal mechanism, with the rate provided by the model's cloud water to rainwater conversion rate. Moist convective scavenging is applied to species that are dissolved within the cloud updraft. The fate of these species follows that of the GCM raindrops: they fall to the surface or are evaporated and returned to the gridbox. We also allow dissolution of the sulfur species following detrainment. We include evaporation and below-cloud scavenging. Evaporation returns an amount of dissolved gas that is proportional to the evaporated water; for the aerosols we divide this amount by 2 unless total evaporation occurs to account for the persistence of the aerosol within larger droplets.

Sulfate is assumed to be fully soluble. The solubility of the carbonaceous aerosols is tuned to give optimal agreement with observations. For organic carbon we use 70% solubility. For black carbon we consider three cases. In case "C" (constant) we use 50% solubility. In case "A" (aged) we assume that black carbon is initially insoluble and transforms to a 90% solubility after a fixed period of time (using an exponential decay time constant of 1.8 days). In case "S" (sulfuric acid coating) we also assume black carbon is initially insoluble but transforms to a 90% solubility in the presence of the gas phase oxidation of SO_2 by OH to form sulfate. We allow up to 10 moles of BC to become soluble for every mole of sulfate produced. The gas-phase sulfate formation occurs during daytime (when OH is available) and is most productive in dry regions and times, since SO_2 will not have been depleted by heterogeneous oxidation. This includes winter because heterogeneous reaction does not occur in frozen water. The solubility amounts (i.e., 50% in case C, 1.8 days in case A, and 10 moles C per mole sulfate in case S) have been chosen so that all cases have comparable global burdens.

In precipitating convective clouds all aerosols are scavenged, except for sulfate detrainment in the cloud anvils and evaporation of aerosols in the falling droplets. Without this assumption we would get excessive carbonaceous loading in the free troposphere. To demonstrate the importance of this assumption, we perform simulation S_{cf}, in which we treat the BC solubility the same as in case S but scavenge only the soluble fraction of BC and OC during convection.

All simulations are done for 3 years, after a 1 year spin-up. For purposes of calculating radiative forcing, we also do a simulation with natural sources only. In the following section, we compare our carbonaceous aerosol results from the year 2000 simulations with observations and with other modeling studies.

3. Model Results: Current Emissions

Table 1 shows the global, annual average budgets for the current-day black carbon simulations. The annual average budgets for the three cases with efficient convective scavenging (cases S, C, and A) are nearly identical. Even though cases S and A are initially insoluble and become soluble later, the relative amounts of removal

Table 1. Black Carbon Aerosol Budgets (Year 2000)

	Case			
	'S'	'A'	'C'	'S_{cf}'
Insoluble Black Carbon				
Sources, Tg C/yr				
Industrial emission	12.41	12.41		12.41
Sinks, Tg C/yr				
Dry deposition	-2.31	-2.38		-2.54
Wet deposition	-2.53	-2.83		-0.40
Insoluble → soluble	-7.57	-7.20		-9.47
Burden, Tg C	0.04	0.04		0.07
Lifetime, days	1.09	1.04		2.00
Soluble Black Carbon				
Sources, Tg C/yr				
Insoluble → soluble	7.57	7.20		9.47
Sinks, Tg C/yr				
Dry deposition	-2.27	-2.14		-2.66
Wet deposition	-5.29	-5.06		-6.81
Burden, Tg C	0.11	0.11		0.22
Lifetime, days	5.42	5.59		8.40
Total Black Carbon				
Sources, Tg C/yr				
Industrial emission	12.41	12.41	12.41	12.41
Sinks, Tg C/yr				
Dry deposition	-4.58	-4.52	-4.54	-5.20
Wet deposition	-7.83	-7.89	-7.87	-7.21
Burden, Tg C	0.15	0.14	0.15	0.29
Lifetime, days	4.40	4.28	4.44	8.42

by dry versus wet deposition are the same as case C (with fixed solubility). Some interesting differences between the insoluble components of cases S and A can be seen in the zonal, annual average mixing ratios, in Figure 1. The insoluble component for case A survives for a fixed amount of time after emission. Case S has a minimum around 30°N where there is abundant gas-phase SO_2 oxidation. Case S also has more transport to the arctic, since the NH winter has low gas-phase oxidation of SO_2 and therefore long-lived insoluble black carbon. This is seen more clearly in January (Figure 2). Note that the NH wintertime burden in case S is also greater (compare contour lines 50, 100, and 200).

Cases S, A, and C differ significantly from the case that does not have efficient convective scavenging (case S_{cf}). In case S_{cf} the only removal of insoluble black carbon is below cloud. Thus more insoluble black carbon survives to become soluble, and the total BC burden and lifetime are double the other cases (Table 1). Figure 3 shows the zonal, annual average mixing ratio for this case, as well as the ratio between cases S_{cf} (Figure 3a) and S (Figure 1a). Without 100% removal in convective updrafts the insoluble BC concentrations in the tropics become quite high. Surface concentrations are nearly the same in the two cases: the total mass in the lowest model is 0.030 Tg C for case S and 0.035 Tg C for case S_{cf}. Even in much of the lower portion of the free troposphere in the Northern Hemisphere the differences are relatively modest (see Figure 3c). The largest differences occur in the upper troposphere. In section 3.1.3 we will see how the different model versions compare with observations in the free troposphere.

The budgets for organic carbon and sulfate are shown in Table 2. As in *Liousse et al.* [1996], we work with organic mass (OM), where OM/OC=1.3, to account for the other elements besides carbon in the compounds. Note that the sulfate lifetime exceeds both carbonaceous aerosols, since the precurser SO_2 more readily escapes to the free troposphere. Wet deposition removes 82% of sulfate, 67% of the OM, and 63% of the BC in the current-day simulations. In the simulation where we do not assume efficient convective scavenging, the OC burden and lifetime increase to 1.12 Tg OM and 4.54 days, respectively. This increase for OC is modest compared with BC, since OC solubility is assumed to be fairly high (70%).

Now we show model results for the mass ratio between carbonaceous and sulfate aerosols. The zonal, annual average of the ratio of BC and OM to sulfate are shown in Figure 4, for current and future emissions. We show only case S since there is little difference between the black carbon simulations. In the zonal av-

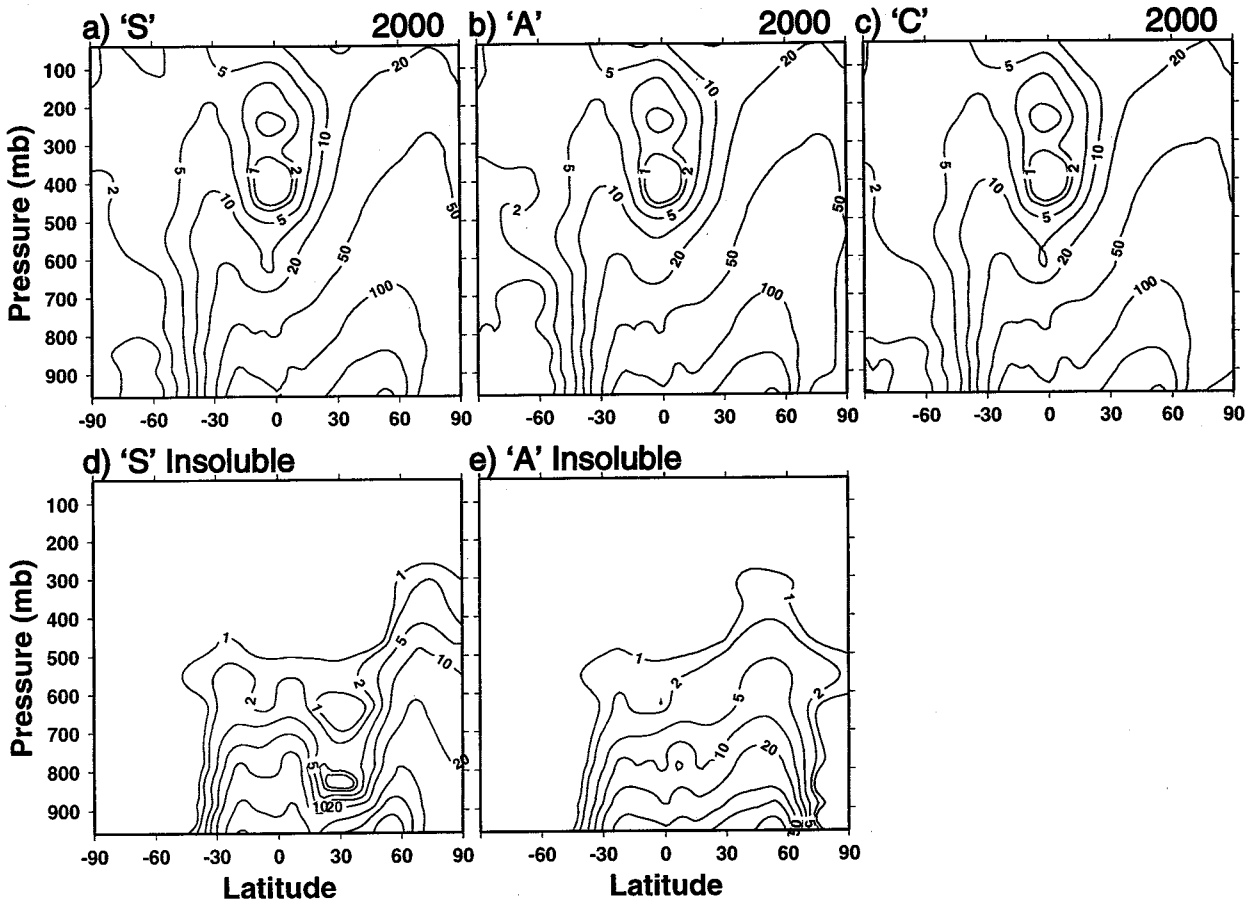

Figure 1. Zonal, annual average black carbon mixing ratio (ng/m^3) in 2000. The top row shows the total mixing ratio for the cases in which solubility (a) depends on exposure to SO_2 oxidation, (b) depends on time, and (c) is constant. The bottom row shows the insoluble component.

erage the ratios decrease with altitude, except south of ~45°S. Organic carbon mass exceeds sulfate in the lower troposphere over biomass burning and industrial regions. Figure 5 shows the map view of these (annual average) ratios for the year 2000, for the column and at the surface. In Europe and Asia, organic carbon is greater than sulfate at the surface. In biomass burning regions, black carbon exceeds sulfate at the surface; organic carbon exceeds sulfate in the column. If we compare the surface and column OM/sulfate ratios, we see that the ratio increases over the Atlantic Ocean. The increase in the model ratio with altitude over the Atlantic and over many other oceanic regions is even greater in summertime, as is shown in Figure 6. The gradient may be attributed at least in part to the natural sulfur source over the oceans, which is greatest in summer. In section 3.1.4, we will compare the model ratio with observations.

3.1. Comparison With Observations

In an attempt to distinguish between the black carbon scavenging mechanisms we compare the model versions with observations. We summarize the performance of the sulfate simulation, examine carbonaceous aerosol surface concentrations, black carbon high-altitude concentrations, the ratio between carbonaceous and sulfate aerosols, and finally consider aerosol seasonality.

We note that comparison of model with carbonaceous aerosol data is hindered by the quantity and quality of available data. Much of the data have duration of only a fraction of a year and some only a fraction of a month. The long-term BC measurements are often inferred from absorption measurements using a constant absorption cross section. *Liousse et al.* [1993] found that the BC absorption cross section varies by a factor of 4 as one moves from source to remote regions. Thus the data in remote regions are especially uncertain.

3.1.1. Sulfate model performance. A detailed evaluation of the sulfate model is given by *Koch et al.* [1999] and is briefly summarized here. Sulfate surface concentrations in North America agree quite well with observations. In Europe the annual average magnitude is good; however, the model tends to produce more seasonality (too much sulfate in summer, too little in winter) compared with observations (a difficulty typical of other sulfur simulations). The sulfur in remote oceanic regions tended to be somewhat too low in the model by *Koch et al.* [1999]; this is improved here because of the

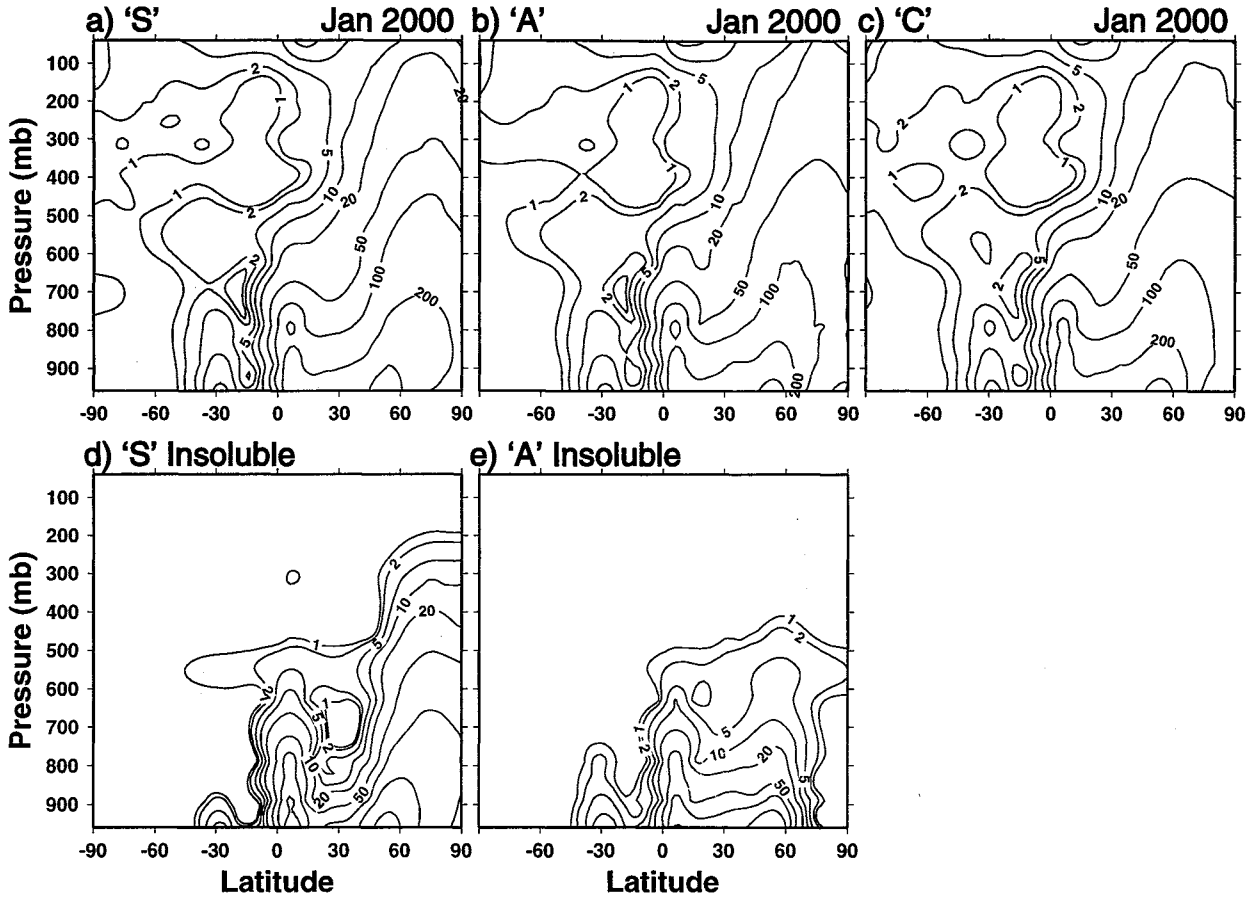

Figure 2. Zonal average black carbon mixing ratio (ng/m^3) in January, as in Figure 1.

higher DMS source. Compared with aircraft and high-altitude observations, the model proved to be somewhat high (though typically within a factor of 2) in polluted regions, and somewhat low in more remote regions.

3.1.2. Carbonaceous aerosol surface concentrations. Figure 7 shows a scatter plot of model versus observed black carbon at the surface for the three scavenging cases, where the model value is the average of the nearest gridbox. Over continents in the Northern Hemisphere, we consider rural sites (NH land-no cities), in addition to all sites (NH land). We do this because the model is unable to capture the very high values in urban areas, perhaps because we do not include supermicron particle emissions, and because the model re-

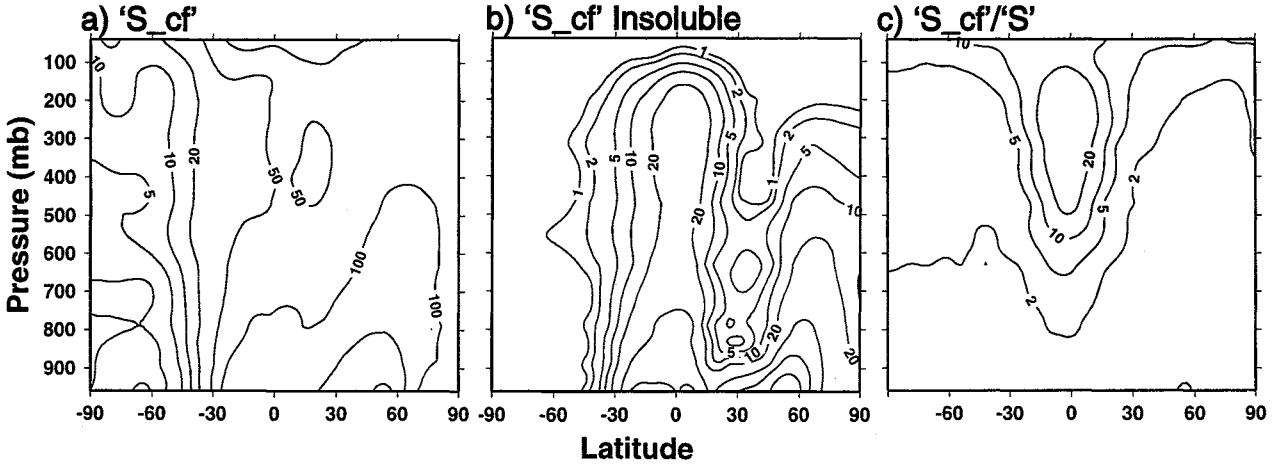

Figure 3. Zonal, annual average black carbon mixing ratio (ng/m^3) in 2000 for (a) the case where solubility depends upon exposure to SO_2 oxidation, without efficient convective scavenging; (b) shows the insoluble part, and (c) shows the ratio of Figure 3(a) to Figure 1(a) (the case with efficient scavenging).

Table 2. Organic Carbon and Sulfate Budgets

	2000	2030	2100
	Organic Carbon		
Sources, Tg OM/yr			
Industrial emissions	81.48	108.72	189.73
Terpene emissions	8.37	8.38	8.38
Sinks, Tg OM/yr			
Dry deposition	-29.75	-38.42	-65.16
Wet deposition	-60.10	-78.42	-132.95
Burden, Tg OM	0.95	1.22	2.16
Lifetime, days	3.86	3.80	3.97
	Sulfate		
Sources, Tg S/yr			
Industrial emissions	2.01	3.26	1.75
Gas phase	14.79	24.40	14.42
Aqueous phase	43.26	57.22	41.69
Sinks, Tg S/yr			
Dry deposition	-10.75	-15.17	-10.18
Wet deposition	-49.31	-69.70	-47.69
Burden, Tg S	0.85	1.28	0.80
Lifetime, days	5.15	5.50	5.03

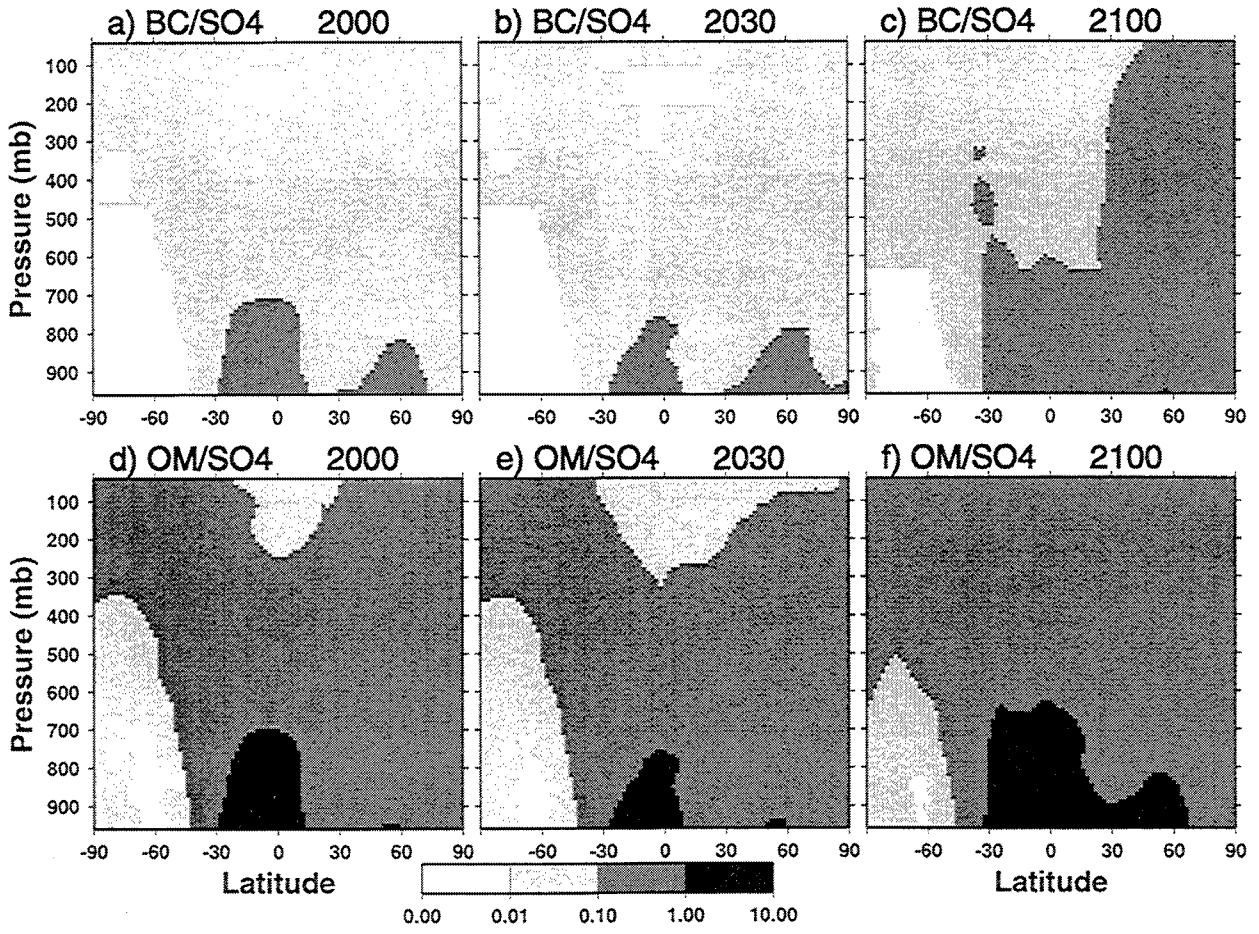

Figure 4. Zonal, annual average ratio of (case S) (top) black carbon and (bottom) organic carbon to sulfate. The columns are for years 2000, 2030, and 2100.

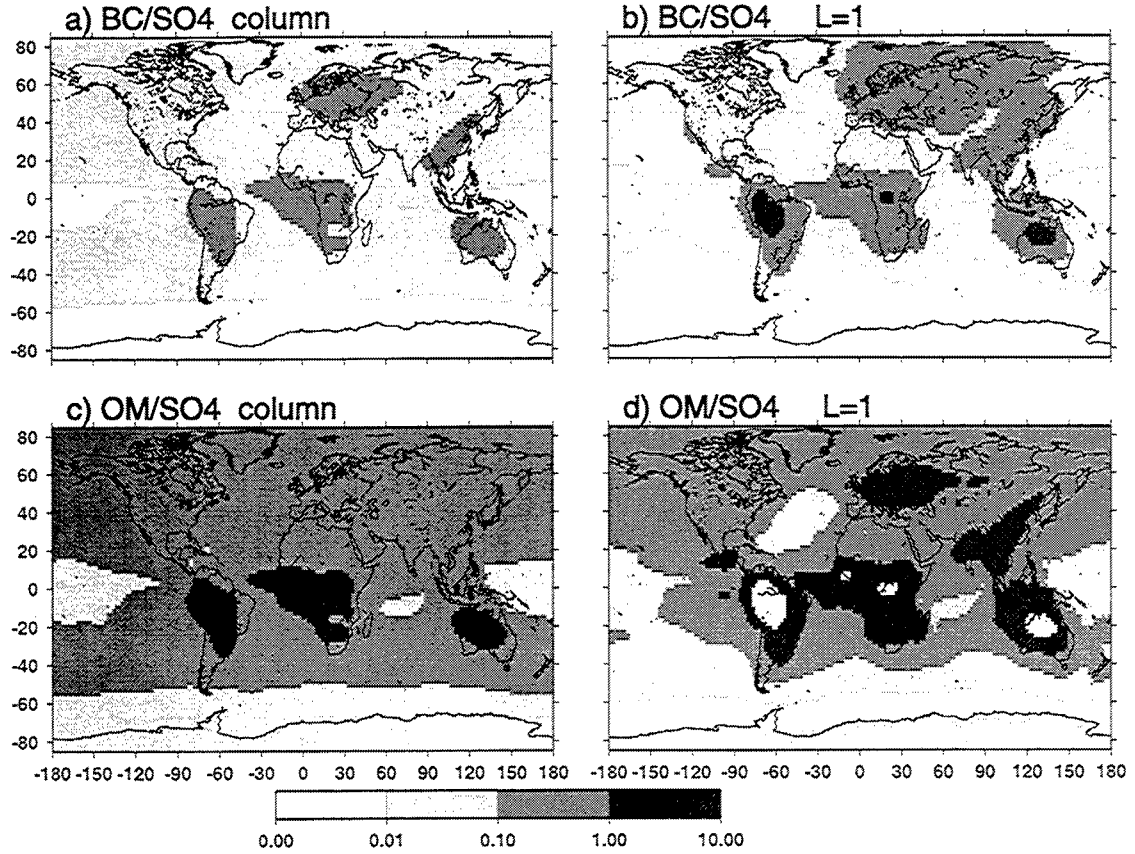

Figure 5. Annual average ratio of (top) black carbon and (bottom) organic carbon to sulfate for the column (left) and in the lowest model layer (right).

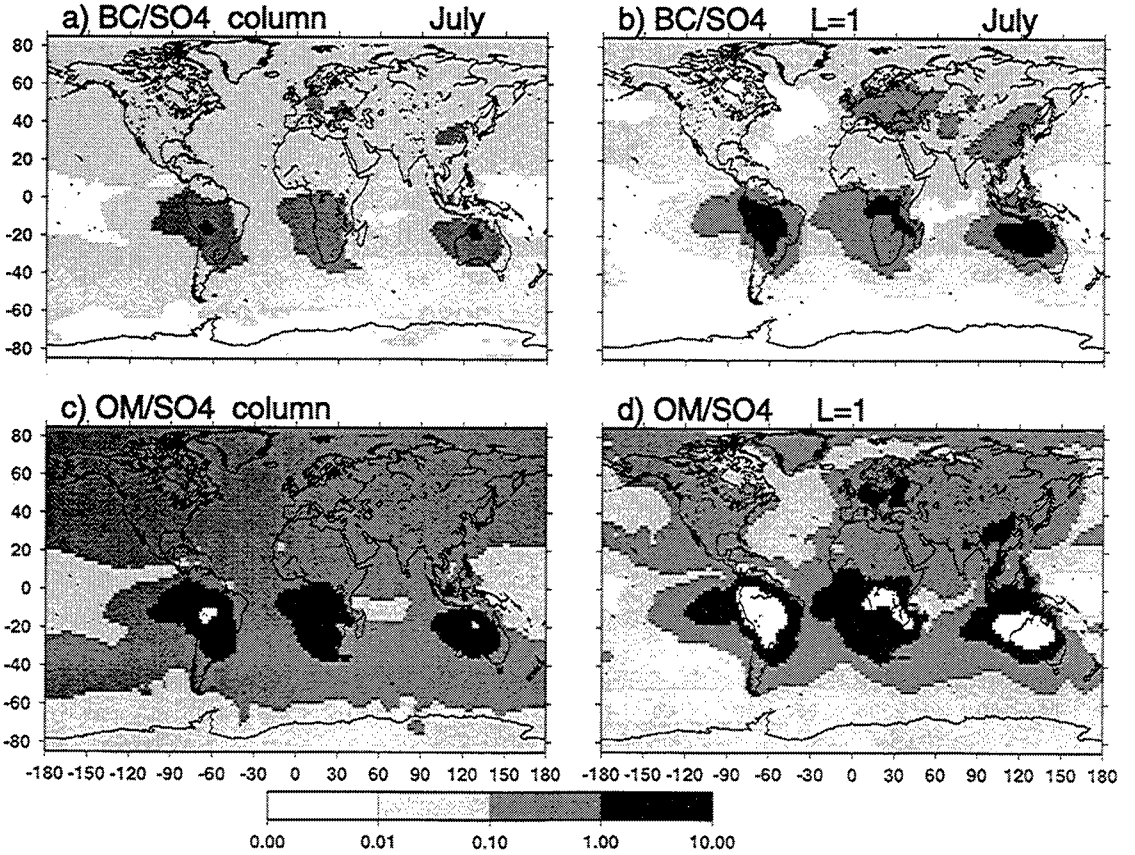

Figure 6. Same as Figure 5, but for July.

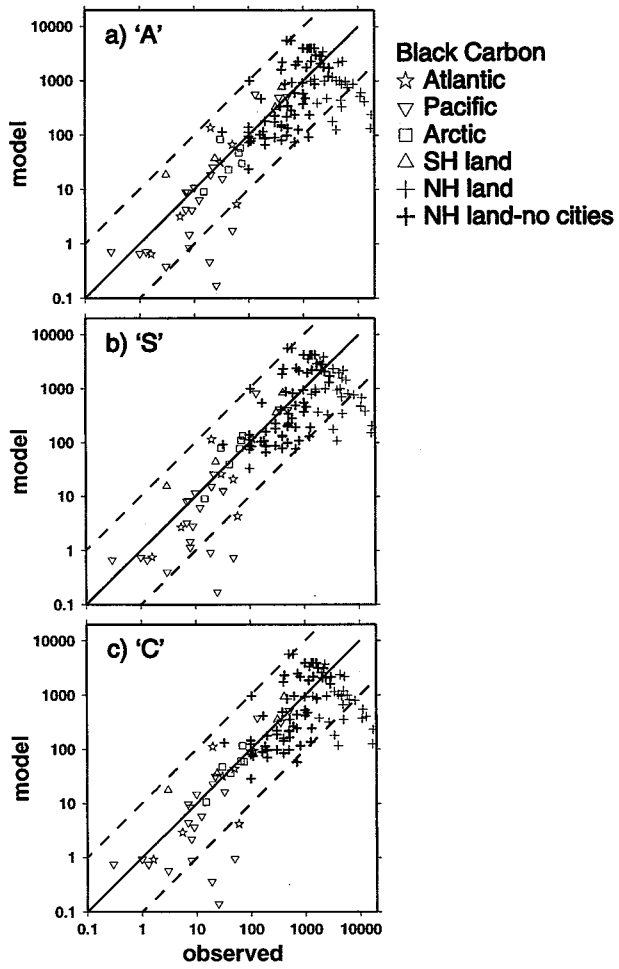

Figure 7. Scatterplot of model versus observed black carbon surface concentrations (ng C/m^3) for the three scavenging scenarios. Dashed lines indicate a factor of 10. Data are compared to the average from the nearest model gridbox. The distinction between urban and rural locations is based on the assessment of *Louisse et al.* [1996], *Cooke et al.* [2000], and T. Novakov (personal communication, 2000). Data are taken from references within *Louisse et al.* [1996] and *Cooke et al.* [2000], and from *Cachier et al.* [1989], *Cadle and Dasch* [1988], *Castro et al.* [1999], *Chow et al.* [1993, 1994], *Davidson et al.* [1988], *Dzubay et al.* [1984], *Heintzenberg and Meszaros* [1985], *Heintzenberg et al.* [1998], *Malm et al.* [1994], *Mólnar et al.* [1999], *Nyeki et al.* [1998], *Ohta and Okita* [1984, 1990], *Pio et al.* [1996], *Smith et al.* [1996], *Valaoras et al.* [1988], *Viisanen et al.* [1989], *Wolff et al.* [1986], and *Wolff and Cachier* [1998].

sults are averages over large gridboxes. The overall bias is minimal (i.e., the scatter is well distributed above and below the zero difference line). Table 3 shows the model biases in different regions, using two different bias definitions: the difference between observations and model (Obs-Mod), and this difference normalized by the observation at each location ((Obs-Mod)/Obs). (Note that the latter definition makes the model look worse when observations are smaller than the model, since we divide a large number by a small one.) If we consider the (Obs-Mod)/Obs bias definition, the model black carbon is generally too high over land, within a factor of 10, and too low in marine regions, within a factor of 2. The model deficiency in remote regions also occurred in the sulfate model and suggests that the model may have insufficient transport from polluted continents to remote regions. The three model versions do not differ greatly in performance, and it is difficult to say that one is best. In the arctic, where the three versions differ the most, the aged (A) black carbon is ~30% too low, indicating that this aging rate causes too much wintertime scavenging; cases S and C agree to within 10%.

Model organic carbon is compared with surface concentrations in Figure 8, with the biases given in Table 3. Observation uncertainties of OM are quite large, similar in magnitude to the measurements themselves in unpolluted regions. This is due to both adsorption of gas phase organics onto the aerosol collection media and to evaporation of volatile species from the aerosol sample. The measurements are also very sparse, with only two measurements in the arctic and three in the Southern Hemisphere over land; very few measurements span a

Table 3. Surface Concentration Model Bias

	Obs-Mod	(Obs-Mod)/Obs
	BC "A"	
Atlantic	5.90	0.19
Pacific	-4.59	0.13
Arctic	17.37	0.32
SH land	-132.07	-2.01
NH land	678.97	-0.59
NH land no cities	-605.14	-0.97
	BC "S"	
Atlantic	0.52	0.21
Pacific	-3.04	0.15
Arctic	-9.50	-0.12
SH land	-154.47	-1.76
NH land	657.58	-0.60
NH land no cities	-627.06	-0.98
	BC "C"	
Atlantic	3.91	0.16
Pacific	0.55	0.08
Arctic	2.66	0.07
SH land	-188.34	-2.05
NH land	684.13	-0.60
NH land no cities	-610.38	-1.00
	OM	
Atlantic	6.98	-0.07
Pacific	483.85	0.45
Arctic	892.76	0.55
SH land	-1542.53	-3.08
NH land	7872.97	0.24
NH land no cities	-1076.68	-0.48

Since most of the data are for less than one year, we weight the biases by the number of months per year represented.

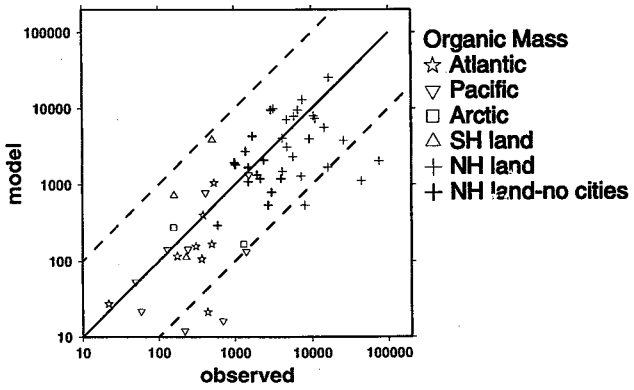

Figure 8. Scatterplot of model versus observed organic mass surface concentrations (ng/m^3). Dashed lines indicate a factor of 10. Data are taken from references listed in Figure 7, and *Hoffman and Duce* [1974, 1977].

full year. The model is somewhat too high over land in the NH (except when compared to urban sites). Model OM is too low over the Pacific, but is in reasonable agreement with observations over the Atlantic.

3.1.3. High-altitude BC concentrations. In order to have some idea of how the model performs at high altitudes, we compare with the few aircraft observations available (in section 3.1.5 we will also compare with two long-term, high-altitude surface measurements). In Figure 9 we compare monthly average model values (of the nearest model gridbox) with the relatively short-duration aircraft measurements. For the sake of clarity, we show only cases S and S_{cf} and note that cases A and C are similar to S. For case S (and A and C) the model is generally too high above 5 km, often by an order of magnitude or more. In the case S_{cf} (without 100% scavenging of BC during moist convection), convective transport carries the unscavenged aerosol to the upper troposphere. Thus, near the top of the troposphere (above 7 km), this case is often more than an order of magnitude higher than the other model cases, making it 2 orders of magnitude or more above the observations. The tropical upper tropospheric observations (points D, E, F, G, and H) are all lower than 2 ng/m^3. If we compare Figures 1a and 3a, we see that the model with efficient convective scavenging (Figure 1a) is much more in accord with the low observed tropical values than the case without efficient convective scavenging (Figure 3a).

However, even with efficient scavenging, there appears to be too much BC in the upper troposphere. Note also that our model does not include an aircraft source, which would increase the disparity further, especially in the flight tracks of the Northern Hemisphere. Besides convective transport, the remaining vertical transport in the GISS model is by eddies, which are not known to be excessive in the GISS model (D. Rind, personal communication, 2000). It is possible that increased vertical resolution in the boundary layer would improve the simulation. Furthermore, the stratiform clouds in this version of the GISS model are located too close to the surface; precipitating clouds at higher altitudes should help to decrease the aerosol concentrations in the free troposphere.

Because of the sparsity of data, this comparison of model with observations is not very reliable; nevertheless, it is important to have some measure of how the model behaves in the free troposphere. High-altitude black carbon, with its absorbing properties, has the potential of significantly altering atmospheric stability. Clearly, more high-altitude carbonaceous aerosol data are needed for model validation.

3.1.4. Ratio between carbonaceous and sulfate aerosols. We now compare the model mass fraction of carbonaceous aerosols to observations. During the TARFOX experiment, which took place in July off the coast of North America, about half the (dry) aerosol

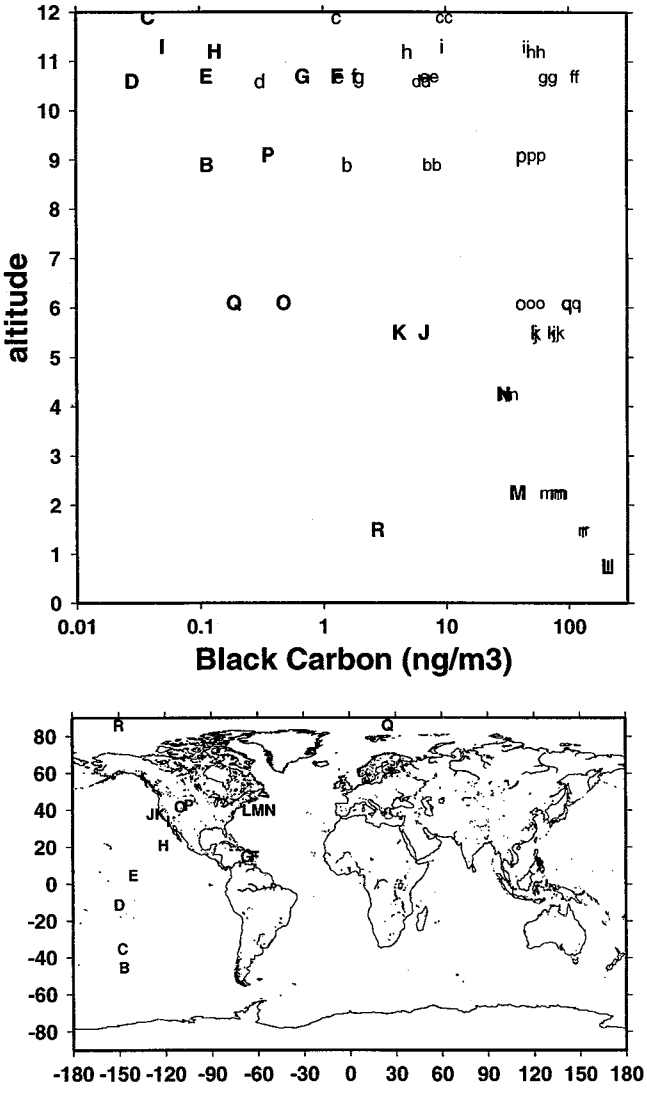

Figure 9. Comparison of model BC (ng/m^3), case S (small letters), case S_{cf} (double small letters) with high-altitude observations (capital letters) from *Pueschel et al.* [1992] and *Blake and Kato* [1995]. Average data uncertainty is ~40%. Data locations are shown below.

Table 4. Comparison of Model and TARFOX Profile

Altitude, km	Observations		Model	
	OM	OM/total	OM	OM/(OM+sulfate)
0.5	6.2	0.26	0.52 (0.51)	0.13 (0.14)
1.2	9.1	0.31	0.52 (0.55)	0.13 (0.15)
2.2	2.9	0.36	0.34 (0.52)	0.12 (0.19)
3.9			0.28 (0.45)	0.14 (0.21)
6.2			0.23 (0.47)	0.17 (0.26)
8.9			0.21 (0.46)	0.18 (0.29)

Units for OM are $\mu g/m^3$. Numbers in parentheses are for the case without efficient convective scavenging. The observed values are based on averages of 35 samples, each of ~15 s duration.

was observed to be carbonaceous, and about half was sulfate; the carbonaceous fraction increased with altitude [*Novakov et al.*, 1997]. In Table 4 we show the data from *Novakov et al.* [1997] averaged over the model layers, compared with the corresponding (monthly average) model values (using the gridbox to the east in order to avoid a gridbox containing land; model results in the three layers above the observations are also shown). In the case of the observations the "total" aerosol was determined gravimetrically; for the model we use the sum of the carbonaceous and sulfate aerosols. The model aerosol is about an order of magnitude lower than observed. This may be because the conditions sampled by TARFOX were more polluted than the monthly average model values; TARFOX sampled in cloudless conditions and tended to seek high aerosol gradients [*Hobbs*, 1999]. The ratio of carbonaceous to total aerosol increases with altitude in the model, but not as steeply as observed. This may be due to the low vertical resolution in the model. Table 4 also shows, in parentheses, the model results for the case without efficient convective scavenging, where the OM loading is higher in the free troposphere. In this case the ratio OM/total increases at nearly the same rate as observed (~40%) between the surface and 2 km.

Now we compare the model ratio of black carbon to sulfate with surface observations where both components are available Figure 10. Most of the data are from the Northern Hemisphere polluted or rural regions. The biases ((Obs-Mod)/Obs) are 0.17, 0.18, and 0.21 for all NH land sites for cases S, A, and C, respectively. If urban sites are excluded, these biases become 0.10, 0.10, and 0.14. Many of these sites are from the IMPROVE data set, from national parks in the United States. At the IMPROVE sites, model sulfate is too high and BC is too low, resulting in a low model bias for the ratio.

3.1.5. Aerosol seasonality. Long-term carbonaceous aerosol records are available at a few locations, allowing us to examine seasonal variability in the model. Some of these sites also have sulfate. Figure 11a-11c shows seasonality at Mace Head, along the western coast of Ireland (350.2°). Mace Head is located just east of the 350° model gridbox boundary. The gridbox in which it falls contains most of Ireland, and has BC concentrations that are higher than the Mace Head observations by more than a factor of 10. The gridbox just west of this contains parts of coastal Ireland and mostly ocean; we show results from this gridbox in Figure 11. All three BC cases give reasonable agreement with observations; case C is probably best, although it is somewhat too low. Note that case S puts too much BC in Mace Head during the winter relative to the summer, suggesting that BC is more soluble in the winter than this model allows.

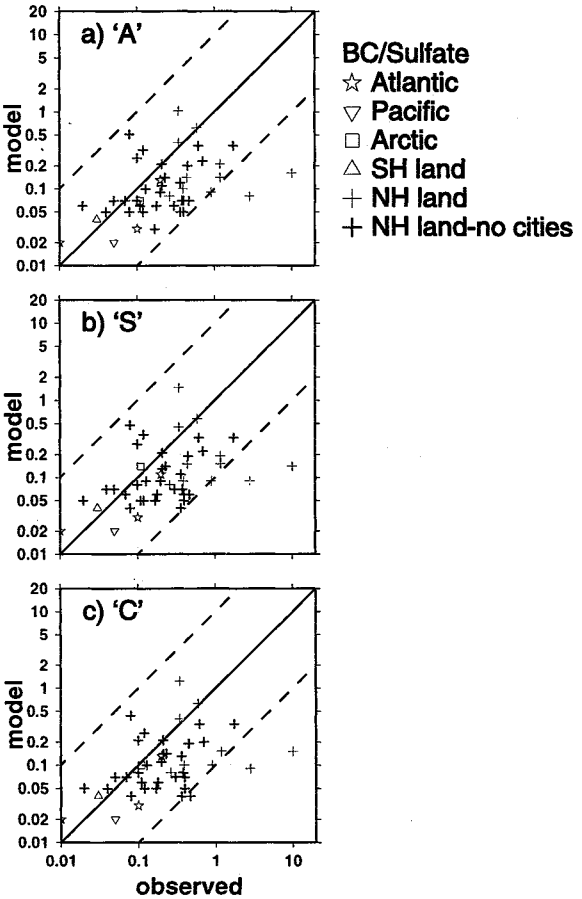

Figure 10. Scatterplot of model versus observed black carbon/sulfate for the three black carbon simulations. Sulfate data are referenced by *Koch et al.* [1999].

Sapporo (Figure 11d-11f) is one of the urban locations where the BC model is much too low due in part to the large model gridbox size, as discussed above. The emissions may also be too low here; *Cooke et al.* [1999] have a somewhat higher emission in this region. The model also has incorrect seasonalities for both BC and sulfate; however the seasonality of the BC/sulfate ratio is roughly correct (Figure 11f). Biases in model precipitation are not a likely cause; if anything, model precipitation in this region is too high in summertime and fairly good in winter. The model sulfate seasonality may suffer from the lack of a wintertime heterogeneous oxidation mechanism, such as the oxidation of SO_2 on seasalt or other particle surface.

We now consider seasonality at high altitude oceanic and continental locations. Figure 11g-11i shows results at Mauna Loa (3400 m). All model versions are reasonably good here, with version S coming closest to achieving the observed springtime BC peak. This peak results from strong westerly transport from Asia and coincides with Asian dust storms. The presence of large amounts of dust may contaminate the absorption measurements from which the BC concentrations are inferred [*Bodhaine,* 1995]. Model transport from Asia may also be deficient.

The BC model is too high at Jungfraujoch (3454 m) (Figure 11j-11l), while the model sulfate is excessive only in summertime. Model version C gives the best

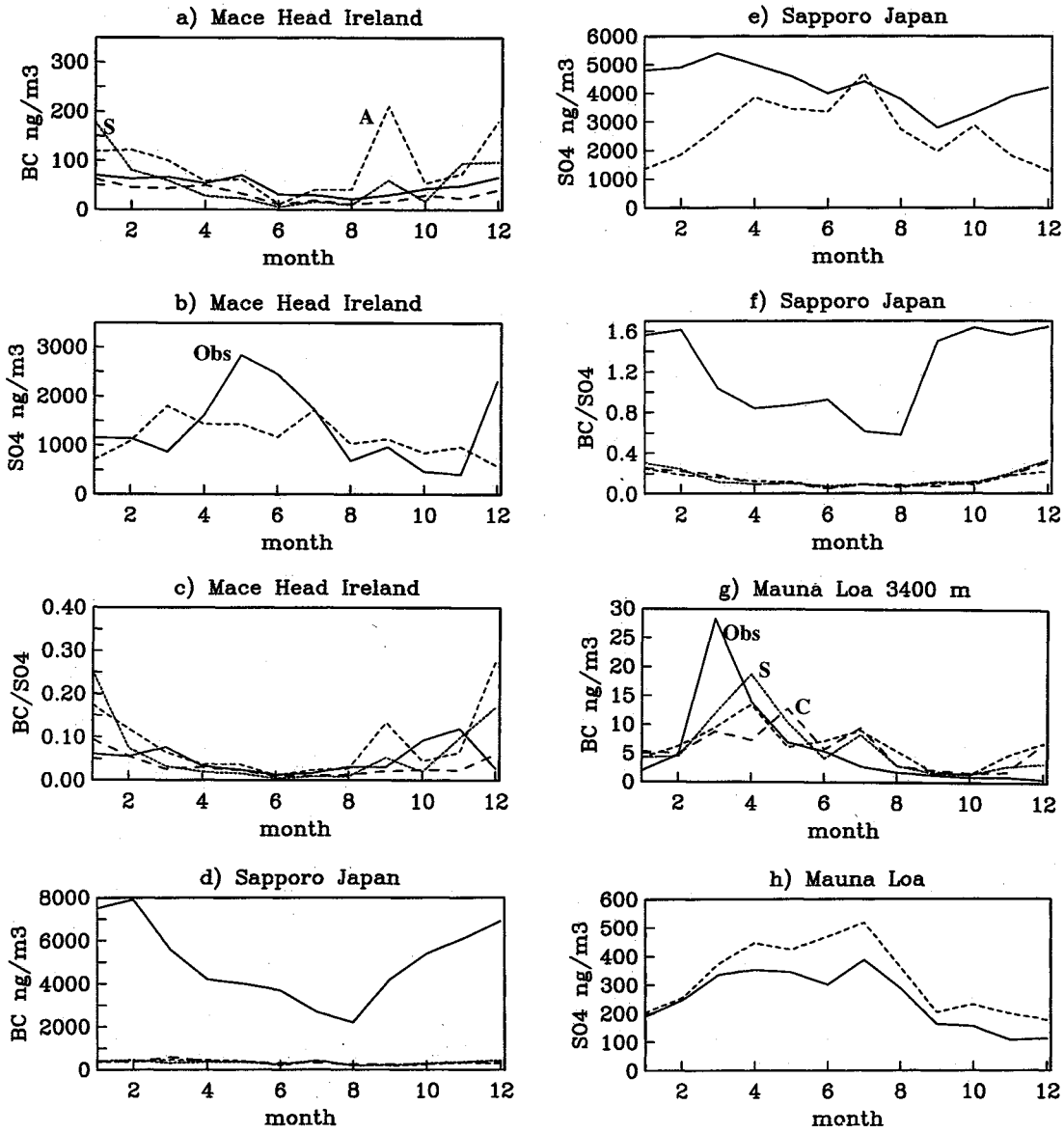

Figure 11. Model and observed seasonal variations of black carbon (a, d, g, h, m, and n), sulfate (b, e, h, and k) and the ratio of the two (c, f, i, and l). Observations are solid, cases S, A, and C are fine, medium, and coarse dashed, respectively. The data at Sapporo are from *Ohta and Okita* [1984, 1990]. Black carbon data at other locations are referenced by *Cooke et al.* [2000] and sulfate is referenced by *Koch et al.* [1999].

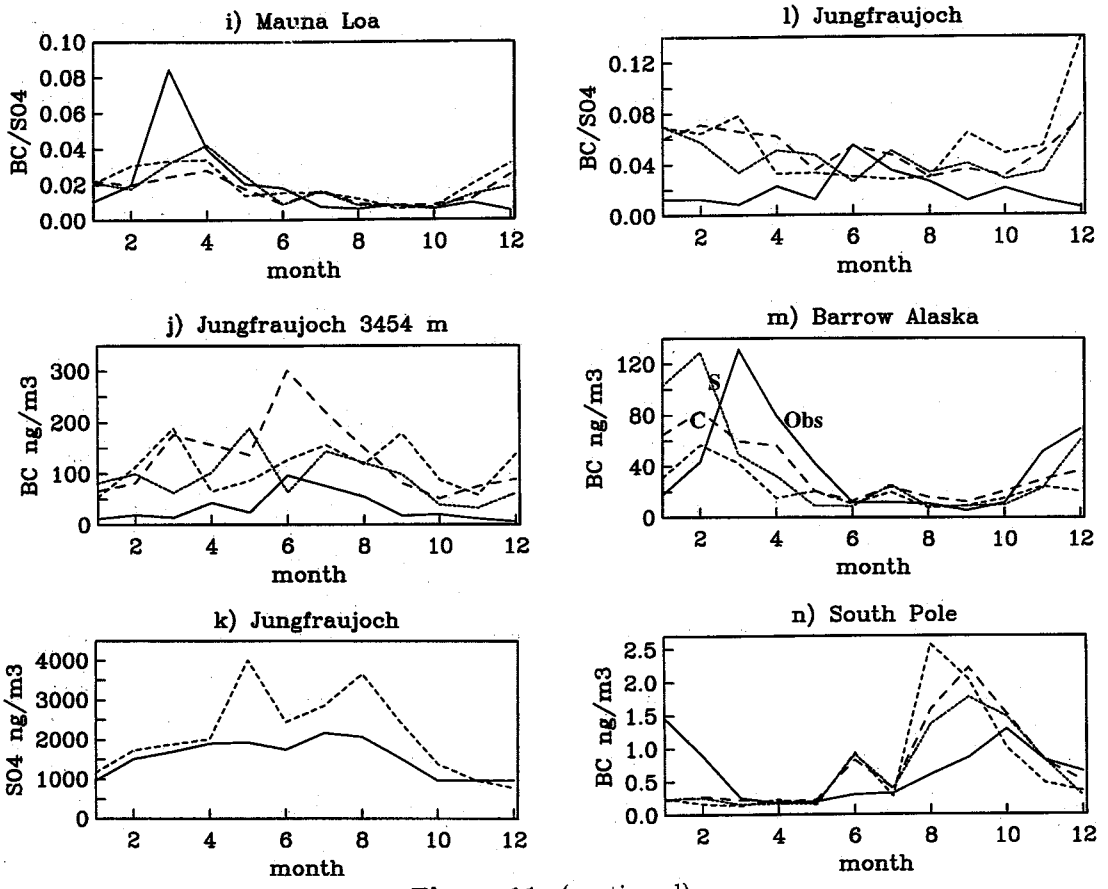

Figure 11. (continued)

BC seasonality, although it also has the largest bias. The BC/sulfate ratio is best in summertime and is too high in winter. It thus seems that we may be missing some removal mechanism for BC in winter and too much lofting or deficient precipitation in summertime.

Black carbon seasonalities at Barrow and the south pole are shown in Figures 11n and 11m. The springtime peak at Barrow occurs one month too early in the model; version S achieves the correct magnitude. Previous model studies have had difficulty getting enough BC at Barrow.

At the south pole, BC peaks in the spring and the summer. The model peaks too early and too high in the springtime and does not peak in the summer. Version S is somewhat better (lower) than the other versions.

3.2. Comparison With Other Models

Our carbonaceous aerosol model is most directly comparable to *Liousse et al.* [1996] (L96), since we use the same sources. In many respects our results are similar. Our BC burden and lifetime are 0.15 Tg C and 4.4 days and theirs are 0.13 Tg C and 4-4.5 days. However, L96 have a greater loss from wet deposition (75%) than we do (64%) (the remaining loss is from dry deposition). This is partly due to the different treatments of dry deposition. L96 used a fixed dry deposition velocity of 0.1 cm/s. This is the same as our global average deposition velocity; however, our resistance in series scheme gives higher dry deposition rates over land, including source regions, typically ~0.15-0.2 cm/s.

Compared with these two studies, *Cooke and Wilson* [1996] (CW96) had a somewhat larger BC source (14 Tg C/yr), and a much higher burden (0.28 Tg C) and lifetime (6-10 days). CW96 use a BC scavenging mechanism like our case A, but with a slightly lower conversion time constant (1.6d, compared with our 1.8d). *Cooke et al.* [1999] (C99) considered only industrial emissions and had lifetimes for OC and BC that are higher than ours (5.3 and 4.5 days, respectively). C99 also used a scavenging mechanism like our case A, but with some aerosol initially soluble, and a shorter time constant (1.2d). Our carbonaceous aerosols have shorter lifetimes than CW96 and C99 because of our efficient scavenging in convection. Note that our case S_{cf}, which does not have the efficient convective scavenging, has a burden of 0.29 Tg C and lifetime of 8.5d, similar to CW96.

The (year 2000) sulfate burden (0.85 Tg S) is somewhat higher than that of Koch et al. [1999] (0.73 Tg S), primarily due to the increased natural DMS source. The burden and lifetime are within the range of previous sulfate models, although they are toward the high end.

Many aspects of the carbonaceous models' perfor-

mances are common. None of the models capture the high concentrations observed at urban sites. This is probably because they all all consider only submicron sized aerosols, and compare gridbox averages with the high values observed near urban centers. All previous models report low BC in the arctic winter and spring, compared with observations. We have shown that a scheme allowing solubility to depend on sulfuric acid coating or a similar scheme allowing dependence on exposure to an oxidating atmosphere, rather than a fixed decay rate, should help in this region. Finally, the tendency to have too much BC in the free troposphere, by at least by an order of magnitude, is also common among the models (although, L96 showed reasonable agreement above a biomass burning location).

4. Model Results: Future Scenario

We saw in the previous section that the BC simulation could be tuned to give minimal overall bias against observations, regardless of the scavenging mechanism. In this section we will see how the different versions behave for projected future emissions in 2030 and 2100. Table 5 shows the BC budgets for these years, and Table 2 shows the budgets for sulfate and OC.

The total S emissions, including natural and anthropogenic sources, are 97 Tg S/yr for 2000, and are projected (in this scenario) to increase to 140 Tg S/yr in 2030 and then decrease below current levels to 89 Tg S/yr in 2100. The BC emissions are 12, 16, and 29 Tg C in 2000, 2030, and 2100, respectively; thus a modest increase is followed by a sharp increase. The OC emission increases are similar to BC. Thus the sulfur/BC emission ratio is 8.1 Tg S/Tg C in 2000, increasing to 8.8 Tg S/Tg C in 2030 and then decreasing to 3.1 Tg S/Tg C in 2100. This allows us to consider a scenario (in 2030) where sulfur is a slightly larger fraction of the anthropogenic emissions, and then a scenario (in 2100) where the sulfur fraction is greatly reduced.

Tables 1, 2, and 5 show that the carbonaceous aerosol lifetimes are slightly lower in 2030 than 2000, even though the emissions increase. This is because the largest emission increases occur in regions where aerosol is relatively efficiently scavenged, such as southeast Asia and eastern Europe. The differences amongst the BC solubility cases remain minor in 2030. The sulfate lifetime increases by ~8%. This is partly because the increased SO_2 load is more likely to deplete the H_2O_2 required for aqueous-phase oxidation, and therefore a greater amount of oxidation occurs in the gas-phase (29% in 2030, compared with ~25% in 2000 and 2100). Since much of the sulfate generated in the aqueous phase is immediately scavenged, an increase in gas-phase production leads to an increase in sulfate burden. However, these shifts in burden are minor, and Figure 4 shows that the zonal average ratio between carbona-

Table 5. Future Black Carbon Aerosol Budgets

	2030 "S"	2030 "A"	2030 "C"	2100 "S"	2100 "A"	2100 "C"
			Insoluble Black Carbon			
Sources, Tg C/yr						
Industrial emission	16.24	16.24		28.83	28.83	
Sinks, Tg C/yr						
Dry deposition	-2.83	-3.09		-7.52	-5.48	
Wet deposition	-2.96	-3.80		-8.95	-6.71	
Insoluble → soluble	-10.45	-9.35		-12.37	-16.64	
Burden, Tg C	0.04	0.05		0.15	0.08	
Lifetime, days	0.98	1.03		1.93	1.03	
			Soluble Black Carbon			
Sources, Tg C/yr						
Insoluble → soluble	10.45	9.35		12.37	16.64	
Sinks, Tg C/yr						
Dry deposition	-3.03	-2.73		-3.48	-4.83	
Wet deposition	-7.42	-6.62		-8.88	-11.81	
Burden, Tg C	0.15	0.14		0.24	0.26	
Lifetime, days	5.13	5.52		7.15	5.75	
			Total Black Carbon			
Sources, Tg C/yr						
Industrial emission	16.24	16.24	16.24	28.83	28.83	28.83
Sinks, Tg C/yr						
Dry deposition	-5.86	-5.82	-5.82	-11.00	-10.31	-10.20
Wet deposition	-10.38	-10.42	-10.42	-17.83	-18.53	-18.63
Burden, Tg C	0.19	0.19	0.19	0.40	0.34	0.36
Lifetime, days	4.28	4.20	4.34	5.00	4.35	4.51

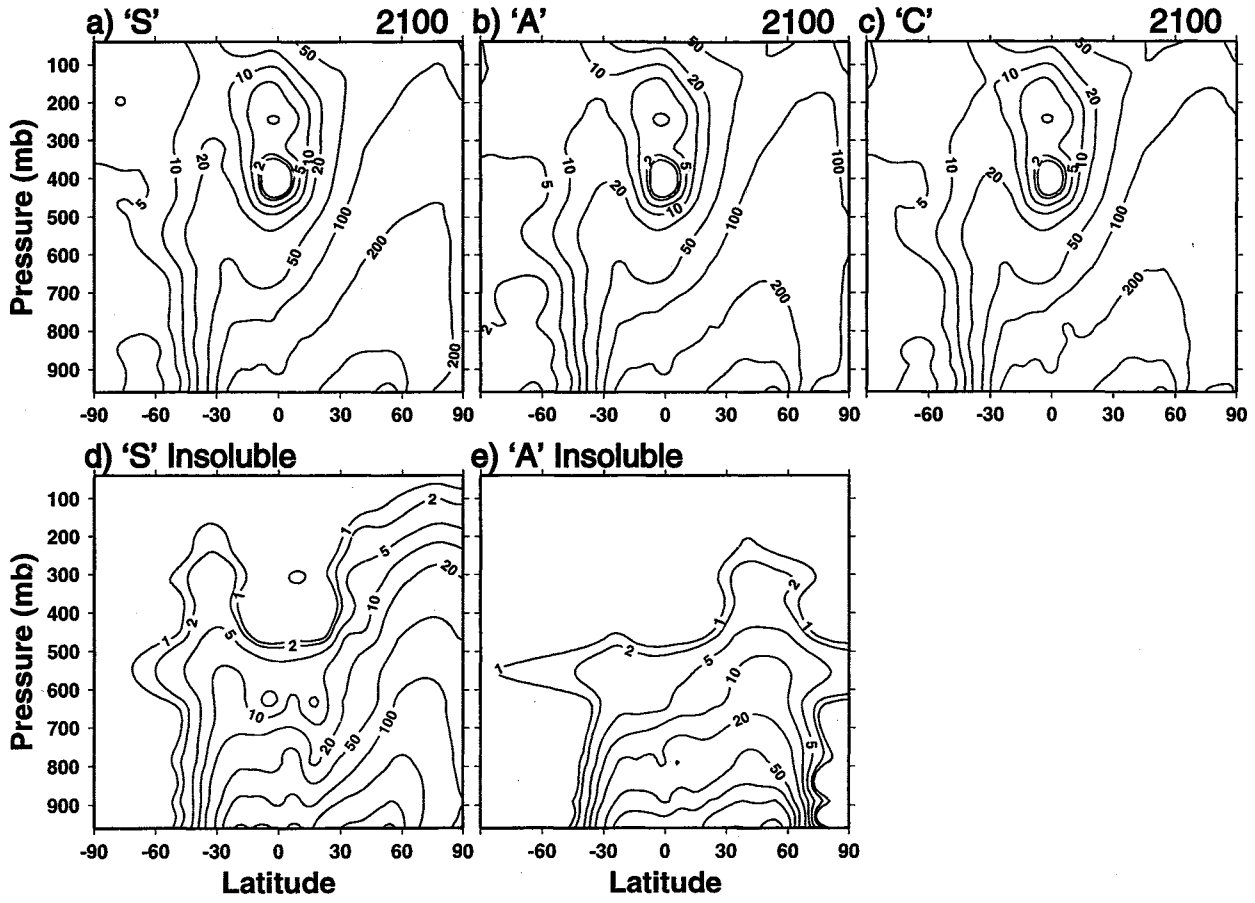

Figure 12. Zonal average BC in 2100 for the three solubility cases. The top row shows the total mixing ratios and the bottom row shows the insoluble component.

ceous and sulfate aerosols is similar in the 2030 and 2000 simulations.

In the 2100 simulations, with the much lower sulfur/BC emission ratio, there is limited SO_2 available to render the case S BC soluble. As a result, the lifetime for insoluble BC in case S doubles. The amount of soluble BC generated in case S is 25% less than in case A, and since more of the soluble BC is generated in dry regions, the soluble component has a longer lifetime in case S compared with case A. The total BC burden and lifetime for case S are now ~10% larger than the other cases. Figure 12 shows the zonal average BC concentrations for each case, along with the insoluble BC contribution. In the Northern Hemisphere, cases A and C are roughly double their levels in 2000 (see Figure 1) and case S is more than double. Case S has insoluble black carbon penetrating higher (and farther) in 2100. Figure 4 shows that in the 2100 simulation, carbonaceous aerosol mass exceeds sulfate in much of the Northern Hemisphere.

The effect of the decreased SO_2 on the BC case S in 2100 demonstrates that in simulations of future aerosol burdens, we need to forecast the changes in the factors affecting aerosol solubility along with the changes in the aerosol emissions. We cannot simply take a fixed insoluble-to-soluble transference rate that has been tuned to the present day and apply it to future climate scenarios. Similarly, we have seen here that

Table 6. Optical Properties at 550 nm

Aerosol Type	Specific Extinction, m^2/g	ω_0	r_{eff}, μm	Optical Thickness
Sulfate	f(RH)[a]	1.00	0.3	0.028
OC	8	0.96	0.5	0.015
BC	9	0.31	0.1	0.003

[a]Dependence upon relative humidity is described by Koch et al. [1999]

the sulfate burden is affected by the availability of oxidants (OH and H_2O_2). In modeling future scenarios the aerosol should be coupled to an atmospheric chemistry code in which the oxidant availability is also permitted to shift.

5. Direct Radiative Forcing

We now consider the radiative forcing of sulfate and carbonaceous aerosols and see how the scattering and absorbing characteristics of the aerosols cause the total aerosol radiative forcing to change as the relative abundances of the aerosol species change.

Aerosol radiative forcing is calculated using the radiation model embedded in the GCM. We summarize the method briefly and refer to *Lacis and Hansen* [1974], *Hansen et al.* [1983], and *Tegen et al.* [2000] for further details. Radiative properties are wavelength dependent and depend upon effective particle size and the wavelength dependent complex refractive indices. They are determined by Mie scattering calculations for the standard gamma size distribution with effective variance 0.2. Optical properties at 550 nm are given in Table 6. Light scattering, absorption, and transmission are calculated using the single Gauss point doubling/adding radiative transfer model. Six K-distribution intervals were used for the spectral dependence of aerosol Mie parameters for the solar part of the spectrum. We calculate the top of the atmosphere direct shortwave radiative forcing due to each species by taking the difference between forcing with and without the species at each radiative time step.

Our approach for calculation of aerosol optical thickness is simple in some respects. We neglect uptake of water by organic or "soluble" black carbon at high relative humidities and instead use specific extinctions that should be applicable for an average relative humidity. We also assume an external mixture of aerosols, even for our case S that would have black carbon encased in sulfuric acid. This will cause an underestimate of black carbon radiative forcing [e.g., *Haywood et al.*, 1997; *Myre et al.*, 1998]. Proper modeling would treat the mixture as an absorbing black carbon core surrounded by a scattering shell. *Jacobson* [2000] has shown that such a treatment increases the BC forcing by 50% (but gives a forcing that is 40% lower than that of a well internally mixed aerosol). To model this properly, one should include a thermodynamic treatment of BC coating in order to know the relative amounts of sulfate and BC and to decrease the sulfate budget by the appropriate amount. We do not attempt this here but note it to be an additional source of uncertainty in the radiative forcing estimates. We also do not consider the indirect forcing of aerosols or impact of dissolved BC on cloud radiative properties.

The direct anthropogenic radiative forcing for each component is shown in Table 7. The anthropogenic forcings for sulfate and OC are found by subtracting the forcings in a preindustrial simulation from the forcings in the simulations with all sources. We calculate BC forcing for the two solubility studies with lowest and highest burdens (cases A and S). Note that for the current and 2030 simulations, the BC and OC forcings nearly cancel one another, on the global average. In the 2100 simulation the BC forcing is larger than the other two components. And for the S simulation, BC is larger than the other two components combined, so that the net aerosol forcing is positive. Since most of the BC increase is projected to occur in the NH, the SH forcing in 2100 is more negative than the NH.

The aerosol radiative forcings are very sensitive to the burdens. We showed in section 3 that for the BC case S_{cf} (the case without efficient scavenging by moist convection), the burden is nearly double the other cases and the burden increase is almost entirely in the free troposphere. The forcing for this case in the 2000 simulation was also about double the other cases, 0.70 W/m^2. Since the case S burden in the free troposphere still appears to be too high, we note that a more accurate model could have a burden and radiative forcing lower by another factor of 2.

The GISS model has a significantly different forcing for clear sky (cloud-free) only, as shown in Table 7. The sulfate and OC forcings are 57 and 47% greater, respectively. The BC forcing is lower by 19%. The resulting total (negative) forcing is 112% larger. As discussed by, e.g., *Haywood and Ramaswamy* [1998], the BC forcing is enhanced when the BC is above a cloud; hence the

Table 7. Anthropogenic Direct Radiative Forcing

	2000				2030			2100		
	NH	SH	Global	(Clear)	NH	SH	Global	NH	SH	Global
Sulfate	-1.16	-0.15	-0.65	(-1.02)	-2.02	-0.46	-1.24	-0.87	-0.21	-0.54
OC	-0.36	-0.23	-0.30	(-0.44)	-0.48	-0.29	-0.38	-0.84	-0.43	-0.64
BC-"S"	0.56	0.13	0.35	(0.19)	0.71	0.17	0.44	2.05	0.43	1.24
BC-"A"	0.60	0.11	0.36		0.80	0.16	0.48	1.53	0.26	0.89
Total ("S")	-0.96	-0.25	-0.60	(-1.27)	-1.79	-0.58	-1.18	0.34	-0.21	0.06
Total ("A")	-0.92	-0.23	-0.59		-1.70	-0.57	-1.14	-0.18	-0.38	-0.29

Forcing is in W/m^2

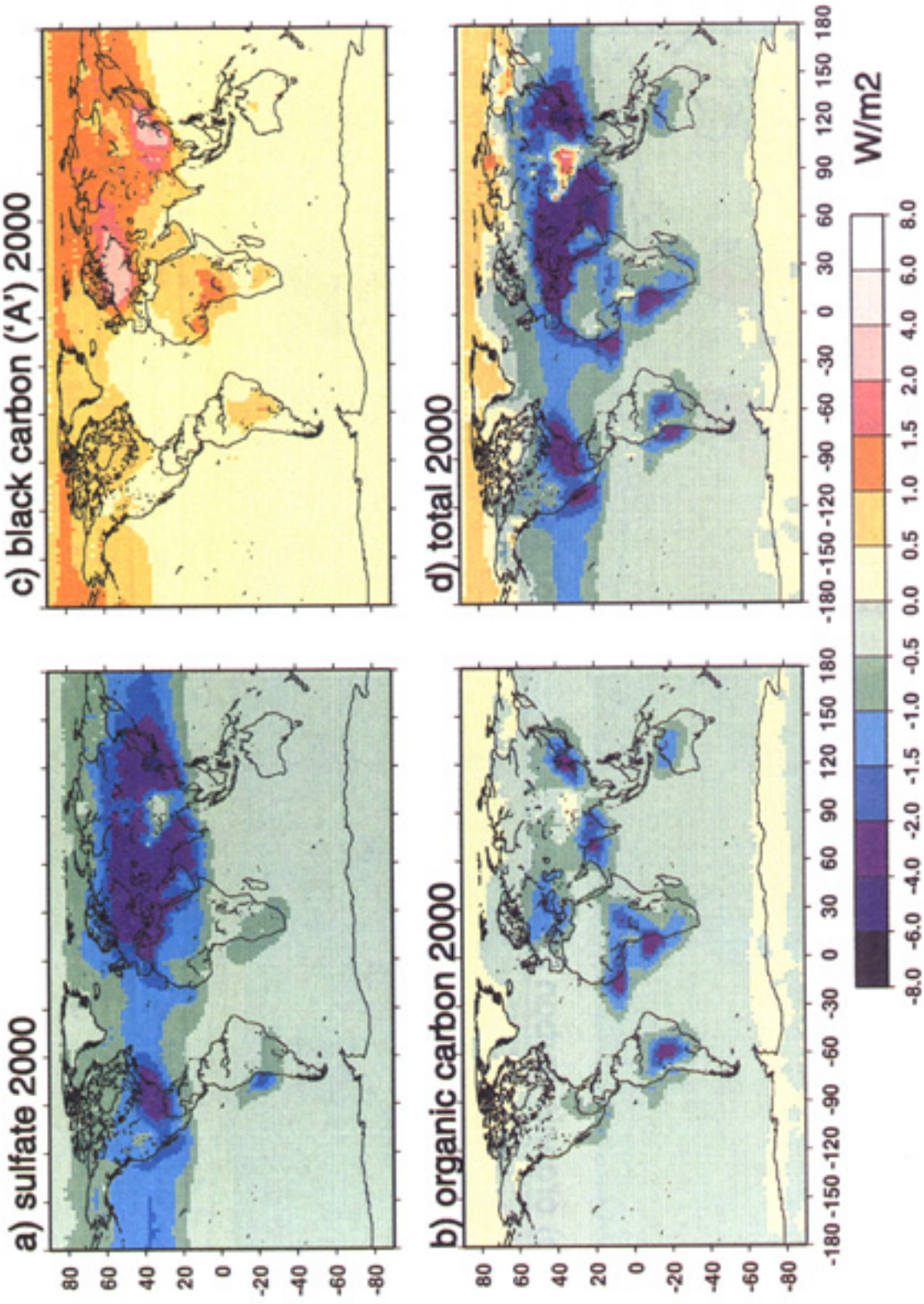

Plate 1. Annual average anthropogenic radiative forcing for (a) sulfate, (b) OC, (c) BC (case A), and (d) total, for the 2000 simulation.

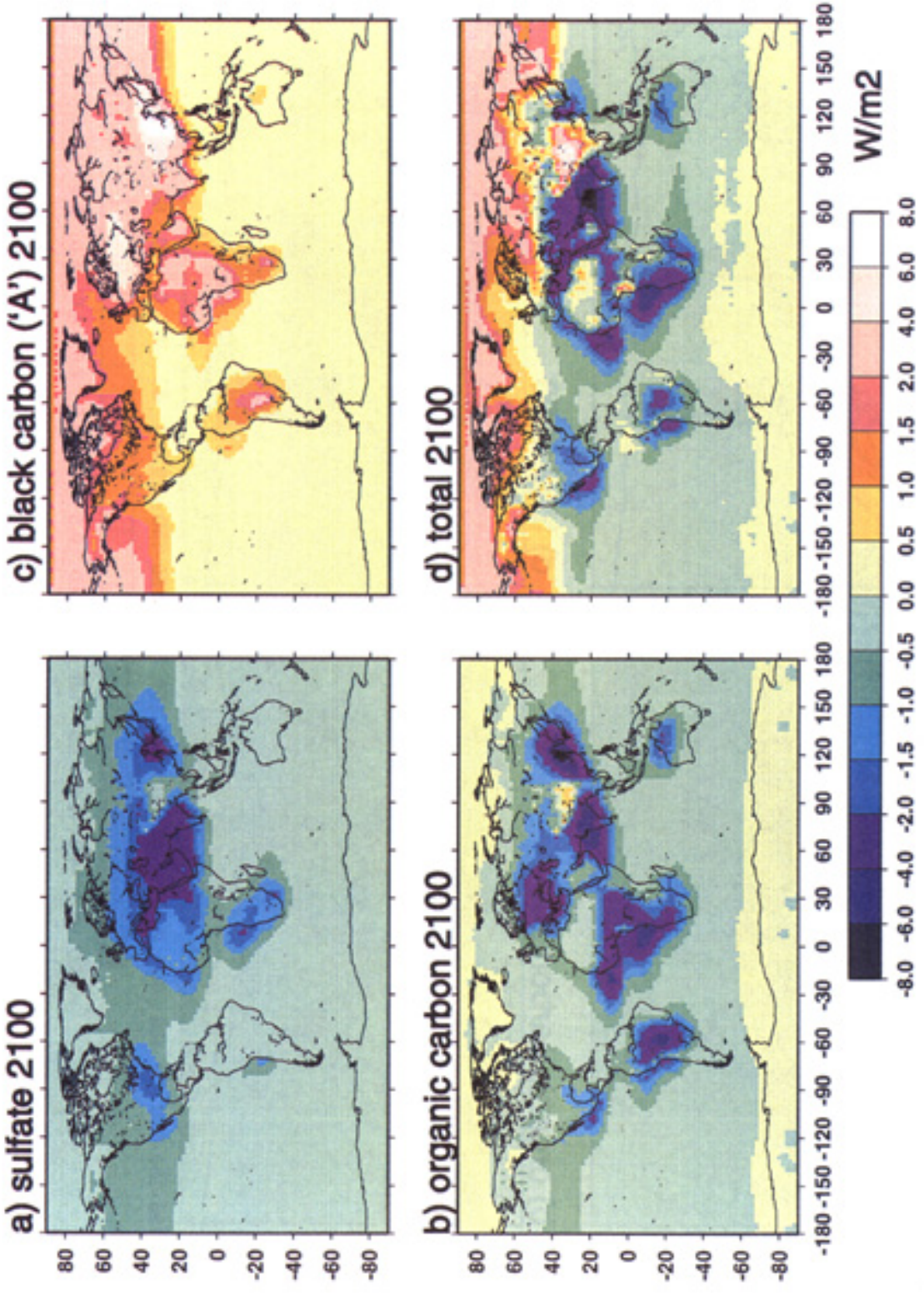

Plate 2. As in Plate 1, for the 2100 simulation.

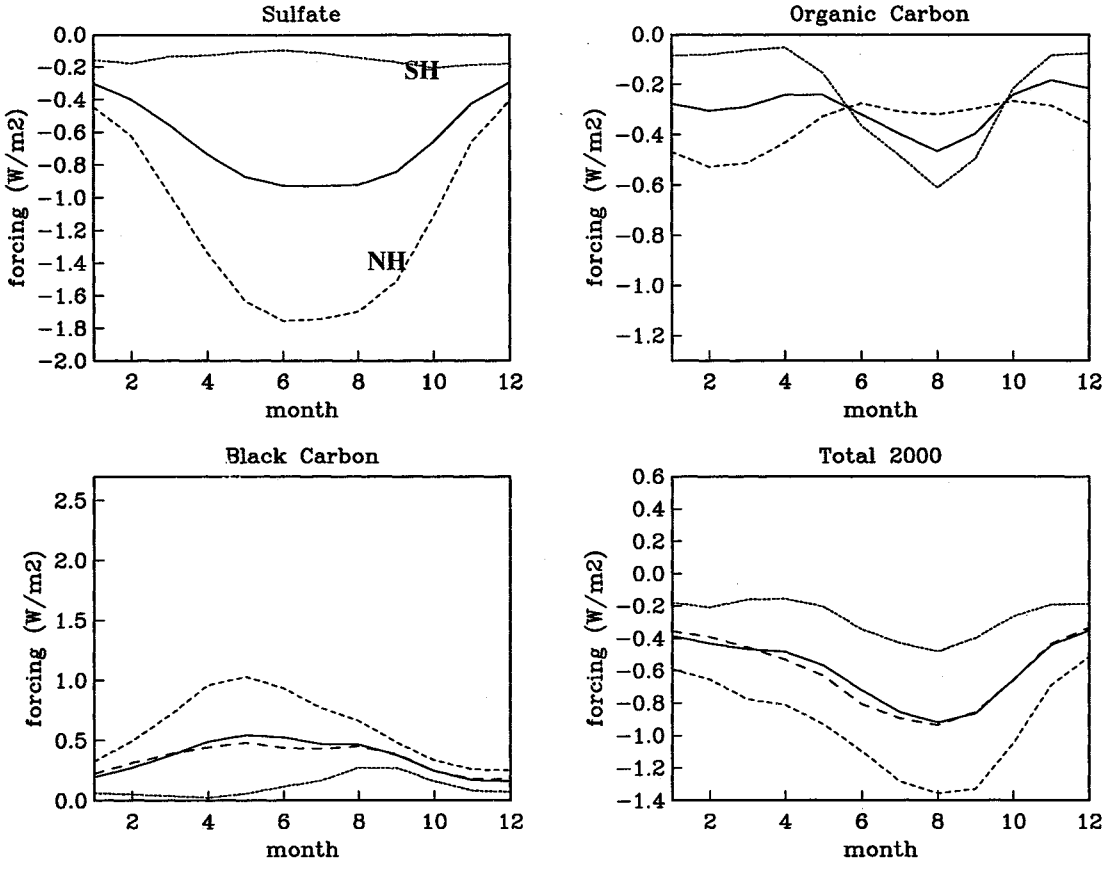

Figure 13. Seasonal variability in 2000 of anthropogenic radiative forcing for sulfate, BC, OC, and the sum of these in the NH (broad dash), SH(small dash), and global average (solid). BC is from case A, but the global average for case S is shown as a broader-dashed line.

increase in forcing when cloudy gridboxes are included.

Plate 1 and Plate 2 show maps of the annual average anthropogenic forcings in 2000 and 2100, respectively. The BC forcing is greatest over eastern Europe and east Asia, with significant forcing throughout Eurasia and much of the arctic. In the 2000 simulation the total aerosol forcing is positive in much of the arctic, becoming negative at mid latitude and low latitude of the NH. The crossover from negative to positive forcing moves considerably southward in the 2100 simulation, to $\sim 40^{\circ}$N. The gradient between the north pole and equator also increases, most dramatically at $\sim 40^{\circ}$E.

Figure 13 and Figure 14 show the seasonal variability of forcing for the three components in the 2000 and 2100 simulations, respectively. We also show the BC forcing for case S. The sulfate forcing is dominated by NH industrial emissions and is maximum in (NH) summertime. The carbonaceous aerosols have a NH springtime industrial peak and a SH biomass burning peak in August. Although the seasonality of each component changes little between 2000 and 2100, the sum of the forcings is quite different for the two periods. In 2000 the net forcing has the same shape as the sulfate forcing, with maximum (negative) forcing occurring in (NH) summertime. However, in 2100 the net forcing seasonality is nearly opposite to what it was in 2000, with summertime forcing close to zero and maximum (negative) forcing occurring in (NH) winter. For case S the aerosol forcing is quite positive in (NH) summertime and would compound rather than counter, greenhouse gas forcing. The shift from aerosols acting as a cooling agent to a heating agent in the (NH) summer could have a dramatic impact on the climate; however, an assessment of the effect requires simulation with variable sea surface temperatures.

We compare our radiative forcing results with other studies that consider both biomass and industrial carbonaceous aerosols. *Haywood and Ramaswamy* [1998] have a stronger forcing for BC, 0.57 W/m^2, when they scale their BC burden (from CW96) to be the same as ours. The higher forcing is probably due to their assumption of a smaller particle size, a geometric mean radius of 0.0118 μm. We use an effective radius of 0.1 μm or a geometric mean radius of $\sim$0.063 μm. According to *Haywood and Ramaswamy* [1998], this increase in particle size would reduce their forcing by $\sim$40%, giving a forcing very close to ours. *Penner et al.* [1998] have a total carbonaceous forcing of -0.07 to 0.04 W/m^2,

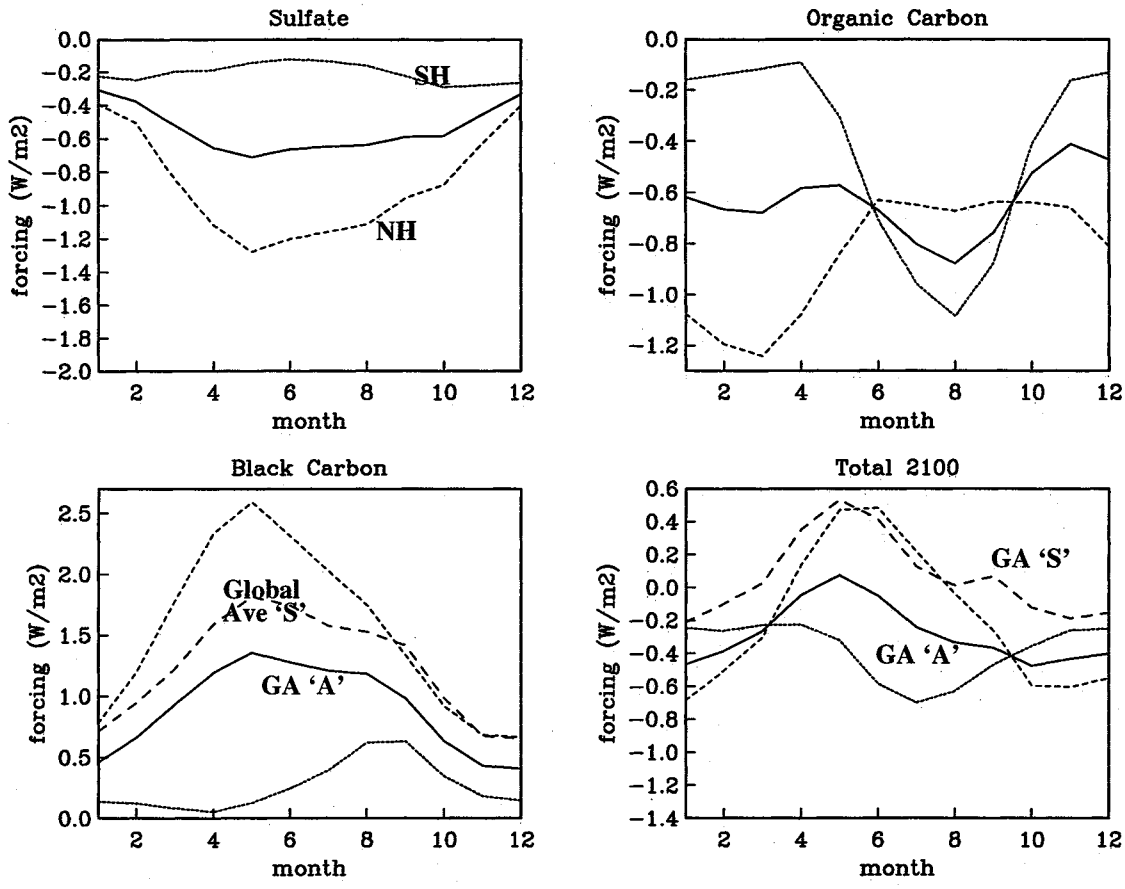

Figure 14. As for Figure 13, but in year 2100.

slightly lower than our result of ~0.05 W/m^2. This may be due to their use of lower specific extinctions, especially for fossil fuel aerosols.

6. Conclusions

We have modeled the transport and direct radiative forcing of the major anthropogenic aerosols: sulfate, black carbon, and organic carbon. The sulfate model is taken from *Koch et al.*, [1999]. The black carbon aerosols were compared with available observations and were typically too low in remote regions (but generally within a factor of 2), were typically too high in continental regions (but generally within a factor of 10), and were typically an order of magnitude or more too high in the free troposphere (above 5 km). The organic mass model was less successful, but typically within a factor of 10 of observations in all regions. The aerosol model performance is similar to previous models.

The BC model results were found to be very sensitive to assumptions about scavenging in moist convection. Without the assumption of 100% convective scavenging of aerosols, the BC burden and radiative forcing double. The surface concentrations are not significantly affected; the increase is almost entirely at high altitudes, especially in the tropics. Thus this scavenging assumption is significant, and it cannot be validated using surface measurements; more high-altitude observations are required.

We have considered the influence of allowing BC solubility to depend upon exposure to gas phase SO_2 oxidation or coating with sulfuric acid. In a sensitivity study we have compared this approach (case S) to two standard approaches: allowing solubility after some fixed aging period (case A), and using a single constant solubility (case C). In each case we tuned the scavenging mechanism to give about the same burden and to give minimal overall bias compared with surface observations. The differences between the three (present day) simulations were minor. The greatest difference was found in the arctic, where case S had higher concentrations in wintertime when gas-phase oxidation of SO_2 is low, BC solubility is reduced, and more BC is transported poleward. Previous models have had difficulty achieving high enough concentrations in polar regions. Thus a solubility mechanism such as sulfuric-acid coating and/or exposure to an oxidizing atmosphere (which is also highest in summer and low in winter) would help increase the polar aerosol concentrations.

Although there is little difference between the current-day simulations, the simulation with sulfur-dependent scavenging gave a 10% higher BC burden and a 40% higher radiative forcing in the IPCC 2100 simulation (which had low SO_2 and high BC emissions) compared

with the other scavenging mechanisms. Of course, the S simulation is a simplified approach, since BC solubility is probably affected by deposition of other gases (such as gas-phase OC), exposure to OH, and physical structure. However, it is illustrative, since none of these elements remain constant. Thus caution should be used in applying a scavenging mechanism that has been tuned to the present observations, to past and future climate studies.

We used our model to study the relative magnitudes of sulfate and carbonaceous aerosols in different regions and altitudes. The carbonaceous aerosols are often comparable to sulfate in the industrial regions of Europe and Asia, and they outweigh sulfate in biomass burning regions. As observed during the TARFOX campaign, the ratio of carbonaceous/sulfate aerosols increased with altitude over the Atlantic ocean. We found this in the model over much of the Atlantic and in some other oceanic regions, especially in the summertime. Over continents and many oceanic regions, however, the ratio decreases with altitude.

We found that the total anthropogenic aerosol direct radiative forcing in current simulations has a distribution and seasonality not dramatically different from sulfate alone. To some extent, BC and OC forcings approximately cancel one another. Net aerosol forcing is smallest in winter and greatest (most negative) in late summer. However, in the 2100 simulation (using the IPCC A2 scenario), BC forcing becomes dominant and the radiative forcing seasonality changes. The north pole-to-equator gradient increases (becomes more positive over the pole and remains strongly negative at lower latitudes). The total average NH forcing becomes positive in summertime and is most negative in winter (a seasonality that is opposite that in the 2000 simulation). This dramatic change in forcing distribution and seasonality warrants more careful modeling in a climate model with a responsive ocean.

Acknowledgments. This work is supported by the NOAA aerosol program. Carbonaceous aerosol observations were largely taken from the compilation of T. Novakov for the NASA GACP program.

References

Bodhaine, B. A., Aerosol absorption measurements at Barrow, Mauna Loa and the south pole, *J. Geophys. Res., 100*, 8967-8975, 1995.

Blake, D. F., and K. Kato, Latitudinal distribution of black carbon soot in the upper troposphere and lower stratosphere, *J. Geophys. Res., 100*, 7195-7202, 1995.

Cachier, H., M.-P. Brémond, and P. Buat-Ménard, Thermal separation of soot carbon, *Aerosol Sci. Technol., 10*, 358-364, 1989.

Cadle, S. H., and J. M. Dasch, Wintertime concentrations and sinks of atmospheric particulate carbon at a rural location in northern Michigan, *Atmos. Environ., 22*, 1373-1381, 1988.

Castro, L. M., C. A. Pio, R. M. Harrison, and D. J. T. Smith, Carbonaceous aerosols in urban and rural European atmospheres: Estimation of secondary organic carbon concentrations, *Atmos. Environ., 31*, 2771-2781, 1999.

Chow, J. C., J. G. Watson, D. J. Lowenthal, P. A. Solomon, K. L. Magliano, S. S. Ziman, and L. W. Richards, PM_{10} and $PM_{2.5}$ compositions in California's San Joaquin Valley, *Aerosol Sci. Technol., 18*, 105-128, 1993.

Chow, J. C., J. G. Watson, E. M. Fujita, Z. Lu, D. R. Lawson, and L. L. Ashbaugh, Temporal and spatial variations of $PM_{2.5}$ and PM_{10} aerosol in the southern California air quality study, *Atmos. Environ., 28*, 2061-2080, 1994.

Cooke, W. F., and J. J. N. Wilson, A global black carbon model, *J. Geophys. Res., 101*, 19,395-19,409, 1996.

Cooke, W. F., C. Liousse, H. Cachier, and J. Feichter, Construction of a 1°x1° fossil fuel emission data set for carbonaceous aerosol and implementation and radiative impact in the ECHAM4 model, *J. Geophys. Res., 104*, 22,137-22,162, 1999.

Davidson, C. I., S.-F. Lin, J. F. Osborn, M. R. Pandey, R. A. Rasmussen, and M. A. K. Khalil, Indoor and outdoor air pollution in the Himalayas, *Environ. Sci. Technol., 20*, 2271-2275, 1988.

Dzubay, T. G., R. K. Stevens, and P. L. Haagenson, Composition and origins of aerosol at a forested mountain in Soviet Georgia, *Environ. Sci. Technol., 18*, 873-883, 1984.

Guenther, A., et al., A global model of natural volatile organic compound emissions, *J. Geophys. Res., 100*, 8873-8892, 1995.

Hansen, J., D. Johnson, A. Lacis, S. Lebedeff, P. Lee, D. Rind, and G. Russel, Climate impact of of increasing atmospheric carbon dioxide, *Science, 213*, 957-966, 1980.

Hansen, J., G. Russell, D. Rind, P. Stone, A. Lacis, S. Lebedeff, R. Ruedy, and L. Travis, Efficient three-dimensional global models for climate studies: Models I and II, *Mon. Weather Rev., 111*, 609-662, 1983.

Haywood, J., and V. Ramaswamy, Global sensitivity studies of the direct radiative forcing due to anthropogenic sulfate and black carbon aerosols, *J. Geophys. Res., 103*, 6043-6058, 1998.

Haywood, J. M., D. L. Roberts, A. Slingo, J. M. Edwards, and K. P. Shine, General circulation model calculations of teh direct radiative forcing by anthropogenic sulfate and fossil-fuel soot aerosol, *J. Clim., 10*, 1562-1577, 1997.

Heintzenberg, J., and E. Mészáros, Elemental carbon, sulfur and metals in aerosol samples at a Hungarian regional air pollution station, *Idojaras, 89*, 313-319, 1985.

Heintzenberg, J., K. Müller, W. Birmili, G. Spindler, and A Wiedensohler, Mass-related aerosol properties over the Leipzig basin, *J. Geophys. Res., 103*, 13,125-13,135, 1998.

Hobbs, P. V., An overview of the University of Washington airborne measurements and results from the Tropospheric Aerosol Radiative Forcing Observational Experiment (TARFOX), *J. Geophys. Res., 104*, 2233-2238, 1999.

Hoffman, E. J. and R. A. Duce, The organic carbon content of marine aerosol collected on Bermuda, *J. Geophys. Res., 79*, 4474-4477, 1974.

Hoffman, E. J. and R. A. Duce, Organic carbon in marine atmospheric particulate material: Concentrations and particle size distribution, *Geophys. Res. Lett., 4*, 449-452, 1977.

Jacobson, M. Z., A physically-based treatment of elemental carbon optics: Implications for global direct forcing of aerosols, *Geophys. Res. Lett., 27*, 217-220, 2000.

Kettle, A. J., et al., A global database of sea surface dimethylsulfide (DMS) measurements and a procedure to predict sea surface DMS as a function of latitude, longitude and month, *Global Biogeochem. Cycles, 13*, 394-444, 1999.

Koch, D., D. Jacob, I. Tegen, D. Rind, and M. Chin, Tropospheric sulfur simulation and sulfate direct radiative forcing in the Goddard Institute for Space Studies general

circulation model, *J. Geophys. Res., 104*, 23,799-23,822, 1999.

Lacis, A. A., and J. E. Hansen, Parameterization for the absorption of solar radiation in the Earth's atmosphere, *J. Atmos. Sci., 31*, 118-133, 1974.

Liousse, C., H. Cachier, and S. G. Jennings, Optical and thermal measurements of black carbon aerosol content in different environments: Variation of the specific attenuation cross section, σ, *Atmos. Environ., 27A*, 1203-1211, 1993.

Liousse, C., J. E. Penner, C. Chuang, J. J. Walton, H. Eddleman, and H. Cachier, A global three-dimensional model study of carbonaceous aerosols, *J. Geophys. Res., 101*, 19,411-19,432, 1996.

Malm, W. C., J. F. Sisler, D. Huffman, R. A. Eldred, and T. A. Cahill, Spatial and seasonal trends in particle concentration and optical extinction in the United States, *J. Geophys. Res., 99*, 1347-1370, 1994.

Molnár, A., E. Mészáros, H. C. Hansson, H. Karlsson, A. Gelencsér, G. Kiss, and Z. Krivácsy, The importance of organic and elemental carbon in the fine atmospheric aerosol particles, *Atmos. Environ., 33*, 2745-2750, 1999.

Myre, G., F. Stordal, K. Restad, and I. S. A. Isaksen, Estimation of the direct radiative forcing due to sulfate and soot aerosols, *Tellus, Ser. B, 50*, 463-477, 1998.

Nakicenovic, N., et al., Emissions scenarios, *A Special Report of Working Group III of the Intergovernmental Panel on Climate Change*, 599 pp., Cambridge Univ. Press, New York, 2000.

Novakov, T., D. A. Hegg, and P. V. Hobbs, Airborne measurements of carbonaceous aerosols on the East Coast of the United States, *J. Geophys. Res., 102*, 30,023-30,030, 1997.

Nyeki, S., U. Baltensperger, I. Colbeck, D. T. Jost, E. Weingartner, and H. W. Gäggeler, The Jungfraujoch high-alpine research station (3454 m) as a background continental site for the measurement of aerosol parameters, *J. Geophys. Res., 103*, 6097-6107, 1998.

Ohta, S., and T. Okita, Measurements of particulate carbon in urban and marine air in Japanese areas, *Atmos. Environ., 18*, 2439-2445, 1984.

Ohta, S., and T. Okita, A chemical characterization of atmospheric aerosol in Sapporo, *Atmos. Environ., 24A*, 815-822, 1990.

Penner, J. E., H. Eddleman, and T. Novakov, Towards the development of a global inventory of black carbon emissions, *Atmos. Environ., 27A*, 1277-1295, 1993.

Penner, J. E., C. C. Chuang, and K. Grant, Climate forcing by carbonaceous and sulfate aerosols, *Clim. Dyn., 14*, 839-851, 1998.

Pueschel, R. F., D. F. Blake, K. G. Snetsinger, A. D. A. Hansen, S. Verma, and K. Kato, Black carbon (soot) aerosol in the lower stratosphere and upper troposphere, *Geophys. Res. Lett., 19*, 1659-1662, 1992.

Pio, C. A., L. M. Castro, M. A. Cerqueira, I. M. Santos, F. Belchior, and M. L. Salgueiro, Source assessment of particulate air pollutants measured at the southwest European coast, *Atmos. Environ., 30*, 3309-3320, 1996.

Rind, D., and J. Lerner, The use of on-line tracers as a diagnostic tool in GCM model development, *J. Geophys. Res., 101*, 12,667-12,683, 1996.

Saxena, P., and L. M. Hildemann, Water soluble organics in atmospheric particles: A critical review of the literature and applications of thermodynamics to identify candidate compounds, *J. Atmos. Chem., 24*, 57-109, 1996.

Smith, D. J. T., R. M. Harrison, L. Luhana, C. A. Pio, L. M. Castro, M. N. Tario, S. Hayat, and T. Quraishi, Concentrations of particulate airborne polycyclic aromatic hydrocarbons and metals collected in Lahore, Pakistan, *Atmos. Environ., 30*, 4031-4040, 1996.

Tegen, I., D. Koch, A. A. Lacis, and M. Sato, Towards a global aerosol climatology: Preliminary trends in tropospheric aerosol amounts and corresponding impact on radiative forcing between 1950 and 1990, *J. Geophys. Res., 105*, 26,971-26,990, 2000.

Valaoras, G., J. J. Huntzicker, and W. H. White, On the contribution of motor vehicles to the Athenian "nephos": An application of factor signatures, *Atmos. Environ., 22*, 965-971, 1988.

Viisanen, Y., J. Hatakka, S. Ahonen, and M. Kulmala, Measurement of particulate carbon in atmospheric aerosol in Helsinki, *Aerosol Sci. Technol., 10*, 224-229, 1989.

Wolff, E. W., and H. Cachier, Concentrations and seasonal cycle of black carbon in aerosol at a coastal Antarctic station, *J. Geophys. Res., 103*, 11,033-11,041, 1998.

Wolff, G. T., M. S. Ruthkosky, D. P. Stroup, P. E. Korsog, M. A. Ferman, G. J. Wendel, and D. H. Stedman, Measurements of SO_x, NO_x and aerosol species on Bermuda, *Atmos. Environ., 20*, 1229-1239, 1986.

D. Koch, NASA Goddard Institute for Space Studies, Columbia University, 2880 Broadway, New York, NY 10025. (dkoch@giss.nasa.gov)

(Received August 8, 2000; revised January 5, 2001; accepted January 17, 2001.)